Aus der Medizinischen Klinik und Poliklinik III
und Helmholtz Zentrum München, Klinische Kooperationsgruppe “Leukämie”
der Ludwig-Maximilians-Universität München,
Direktor: Prof. Dr. med. Wolfgang Hiddemann

Expression Analysis of the *OSTL* Gene in Leukemia Patients

Dissertation
zum Erwerb des Doktorgrades der Medizin
an der Medizinischen Fakultät der
Ludwig-Maximilians-Universität zu München

Vorgelegt von
Anna Sophia Japp
Frankfurt am Main

München
2013

Mit Genehmigung der Medizinischen Fakultät der Universität München

Berichterstatter:	Prof. Dr. med. Stefan K. Bohlander
Mitberichterstatter:	Priv. Doz. Dr. Christian Ries
	Priv. Doz. Dr. Irmela Jeremias

Dekan:	Prof. Dr. med. Dr. h.c. M. Reiser, FACR, FRCR

Tag der mündlichen Prüfung: 17.10.2013

Contents

1 Introduction

1.1 Leukemia

Cancer is one of the leading causes of death worldwide. In 2004 approximately 13 % of all human deaths were due to cancer (WHO, 2009). Leukemia accounts for about 3.8 % of all cancer deaths (CD Mathers, 2001).

Leukemia can be divided into lymphoid and myeloid leukemia. These expressions characterize the lineage the malignant cells originate from (SH Swerdlow, 2008).

Furthermore, leukemic disorders can be divided into acute and chronic forms. Acute leukemia leads to death in as short a time as days or weeks, if untreated. This is caused by differentiation arrest, which leads subsequently to an excess of immature cells in the bone marrow, as well as in the peripheral blood. Chronic leukemia may lead to death within months or years. It is also characterized by an overbalance of one hematopoietic cell line. The cells however show a more mature differentiation (SH Swerdlow, 2008).

In the following section I will briefly describe the main types of leukemia that are relevant to this study (AML, ALL, CML).

1.1.1 Acute Lymphoblastic Leukemia (ALL)

Acute Lymphoid Leukemia or Acute Lymphoblastic Leukemia is characterized by an excess of immature lymphocytes that may accumulate in the bone marrow and sometimes in the peripheral blood (RF Cornell, 2012). The disease is more common in children than in adults. The median age at diagnosis is 13 years, whereas the peak incidence is between the ages of 2 to 10 years. 80 % of childhood leukemia is diagnosed as ALL. The total incidence (all ages) is approximately 2/100.000/year (JF Yamamoto, 2008). ALL is considered as acute leukemia due to the relatively short course leading to death if untreated. The symptoms are related to the progression of bone marrow suppression or organ infiltration. If treated in time, the prognosis of ALL is generally positive with a cure rate of more than 80 %, however, in the case of relapse, the prognosis is rather

adverse. Genetic abnormalities are found to be important prognostic factors and should be taken into account, when diagnosing ALL (NL Harris, 2000). Table 1.1 demonstrates the relation of prognosis and cytogenetic alterations (RW McKenna, 2000).

Prognosis of ALL related to cytogenetics	
Favorable	Hyperdiploidy >50 cryptic t(12;21)(p12;q22)
Intermediate	Hyperdiploidy 47-50 Normal (diploidy) del(6q)
Unfavorable	Hypodiploidy: near haploid near tetraploid del17p t(9;22)(q34;q11) t(11q23), usually t(4;11)

Table 1.1: This table shows the correlation between cytogenetic features and the clinical prognosis. Adapted from RW McKenna, 2000.

There are two main classifications for ALL. The former commonly used classification is the FAB (French-American-British) classification (see Table 1.2). It was first proposed in 1976 and is based on the phenotype of the leukemic cells. But the morphological categorization does not show prognostic relevance. On the other hand this classification is easy to use because no advanced technologies are needed (RW McKenna, 2000).

FAB classification of ALL			
	L1	**L2**	**L3**
Cell size	Small	Large, often heterogeneous	Large, homogenous
Amount of cytoplasm	Scant	Moderately abundant	Moderately abundant
Nucleoli	Inconspicuous	Prominent	Present, may be prominent
Cytoplasmatic vacuoles	Variable	Variable	Prominent

Table 1.2: This table displays the classification criteria of the French-American-British Classification. They are based on morphologic and cytochemical features. Adapted from RW McKenna, 2000.

WHO classification of ALL
Precursor B-cell acute lymphoblastic leukemia (cytogenetic subgroups) t(9;22)(q34;q11) *BCR/ABL* t(v;11q23) *MLL* rearranged t(1;19)(q23;p13) *E2A/PBX1* t(12;21)(p12;q22) *ETV/CBF*α
Precursor T-cell acute lymphoblastic leukemia
Burkitt cell leukemia

Table 1.3: The table shows the classification of acute lymphoblastic leukemia by the World Health Organization. Adapted from NL Harris, 2000.

The World Health Organization (WHO) developed a new classification in 2001 (see table 1.3). It includes cytochemistry, immunophenotyping, genetics and clinical features, in addition to morphology (JW Vardiman, 2009). This ensures prognostic information and has a great impact on the determination of the appropriate treatment.

1.1.2 Acute Myeloid Leukemia (AML)

Acute Myeloid Leukemia, also known as Acute Myelogenous Leukemia, is characterized by a clonal proliferation of myeloid precursors who have a reduced capacity to differentiate between e.g. granulocytes or monocytes. These immature leukemic blasts can accumulate in the bone marrow, peripheral blood and other organ tissues. This causes symptoms varying according to the infiltration (RF Cornell, 2012).

AML is more common in adults. It accounts for about 80 % of acute leukemia in adults. The median age at diagnosis is 65 years. The incidence of AML increases with age, but the total incidence remains relatively stable at approximately 3-5/100.000/year over the years. AML is slightly more common in men with a male: female ratio of 5:3 (JF Yamamoto, 2008).

An important factor for the prognosis is cytogenetics. Table 1.4 displays the relationship between 5-year survival and cytogenetic abnormalities (K Wheatley, 1999).

Risk Category	Cytogenetic abnormality	5-year survival
Favorable	t(8;21), t(15;17), inv(16)	70 %
Intermediate	Normal, +8, +21,+22, del(7q), del(9q), Abnormal 11q23, all other structural or numerical changes	48 %
Adverse	-5, -7, del(5q), Abnormal 3q, Complex cytogenetics	15 %

Table 1.4: This table shows the correlation of certain cytogenetic alterations and their prognosis. Adapted from K Wheatley, 1999.

The FAB classification of AML, as well as for ALL, is the most commonly used classification. This classification divides AML into eight subtypes (M0-M7) based mainly on morphological features of the leukemic cell (see Table 1.5; RW

McKenna, 2000). Though still frequently used, the WHO classification offers a more useful categorization due to its diagnostic, prognostic and therapeutic relevance (JW Vardiman, 2009). Table 1.6 gives an overview of the WHO classification.

FAB classification of AML	
M0	Myeloblastic leukemia minimally differentiated
M1	Myeloblastic leukemia without maturation
M2	Myeloblastic leukemia with maturation
M3	Hypergranular promyelocytic leukemia Microgranular variant
M4	Myelomonocytic leukemia With bone marrow eosinophilia (M4E0)
M5	Monocytic leukemia Poorly differentiated (M5A) Differentiated (M5B)
M6	Erythroleukemia
M7	Megakaryoblastic leukemia

Table 1.5: Subgroups of AML characterized by the French-American-British Classification. Adapted from RW McKenna, 2000.

WHO Classification of AML
I. AML with recurrent cytogenetic translocations AML with t(8;21)(q22;q22), *AML1(CBFα)/ETO* Acute promyelotic leukemia with t(15;17)(q22;21) and variants, *PML/RARα* AML with abnormal bone marrow eosinophils inv(16)(p13;q22) or t(16;16)(p13;q22), *CBFβ/MYH11X* AML with 11q23 (*MLL*) abnormalities
II. AML with multilineage dysplasia With prior myelodysplastic syndrome Without prior myelodysplastic syndrome
III. AML and myelodysplastic syndrome, therapy related Alkylating agent related Epipodophyllotoxin related Other types
IV. AML not otherwise categorized AML minimally differentiated AML without maturation AML with maturation Acute myelomonocytic leukemia Acute monocytic leukemia Acute erythroid leukemia Acute megakaryocytic leukemia Acute basophilic leukemia Acute panmyelosis with myelofibrosis

Table 1.6: Classification of AML by the World Health Organization (WHO). Adapted from NL Harris, 2000.

1.1.3 Chronic Myeloid Leukemia (CML)

Chronic Myeloid Leukemia or Chronic Myelogenous Leukemia (CML) mostly presents with elevated white blood cell count with left shift, often with basopilia, and an enlarged spleen. Many patients display no symptoms or non-specific symptoms like malaise, fever or anemia on diagnosis (J Cortes, 2012; NF Grigoropoulos, 2013). CML can affect individuals at any age, although the majority is middle-aged or elderly on diagnosis. The incidence is 1-2/100.000/year with a slight predominance of men over women (JF Yamamoto, 2008). CML accounts for 20-30 % of all leukemia in adults. The course of the disease can be divided into three phases, starting with the chronic phase that may last for years.

The disease continues to the acceleration phase and terminates with the blast crisis.

Acceleration phase of CML
10–19% blasts of peripheral blood cells or bone marrow cells >20% basophiles in the peripheral blood
Persistent thrombocytopenia (<100 x 10^9/L) unrelated to therapy, or persistent thrombocytosis (>100 x 10^9/L) unresponsive to therapy
Increasing spleen size and increasing WBC count unresponsive to therapy
Cytogenetic evidence of clonal evolution (i.e., the appearance of an additional genetic abnormality that was not present in the initial specimen at the time of diagnosis of chronic phase CML)

Table 1.7: The WHO characterizes the acceleration phase of CML as displayed in this table. Adapted from JW Vardiman, 2002.

Any of the characteristics mentioned in Table 1.7 may be an indicator for a progress of the disease to the acceleration phase. It is of great importance to recognize this development because, in this stage, a blast crisis is of a much higher risk. The blast crisis behaves similarly to acute leukemia and shows a rapid turnover of the cells. The progression can be diagnosed if any of the following is present:

Criteria for blast phase
>20% blasts of peripheral blood cells or bone marrow cells
Extramedullary blast proliferation
Large foci or clusters of blasts in the bone marrow biopsy

Table 1.8: The table displays the criteria to diagnose a blast crisis in patients with CML. Adapted from JW Vardiman, 2002.

1.2 Genetics and leukemia

1.2.1 Basis of tumor genetics

1.2.1.1 Tumor suppressor gene:

Tumor suppressor genes are genes that have an influence on cell cycle control, e.g. inhibition of cell proliferation. More precisely, they encode for proteins that are involved in regulation of progression through certain stages of the cell cycle (e.g. Rb), checkpoint-control proteins that lead to cell cycle arrest, if the DNA is damaged (e.g. p53), proteins that promote apoptosis or DNA repair enzymes (H Lodish, 2007). If these genes are altered in their function, the cell cycle regulation is disturbed. This leads to uncontrolled proliferation, although the DNA is already damaged. Further mutations can accumulate under these conditions and contribute to the development of hematopoietic malignancy. This principle of oncogenesis is known as “Loss of Function” (WS Klug, 2005).

The inactivation of a tumor suppressor gene can take place due to mutations, deletions, as well as inversions and translocations, which result in an inoperable gene (T Burmeister, 2000).

Mostly it is not sufficient that only one allele is altered to cause malignant transformation. Knudson’s “Two-hit” hypothesis points out that both alleles of a tumor suppressor gene have to be inactivated to initiate tumor development (AG Knudson, 1971).

TP53 is the most popular example of a tumor suppressor gene.

1.2.1.2 Proto-oncogene:

Proto-oncogenes usually have an important role in cell physiology. Genetic alterations can transform a proto-oncogene into an oncogene. A “gain of function” mutation is needed for this process (H Lodish, 2007). Such mutation could be amplification of a DNA segment that holds a proto-oncogene and subsequently leads to overexpression of the encoded gene. Alternatively, the proto-oncogene comes under the control of a different promoter or enhancer, which also leads to overexpression of the oncogene. Another possibility would be balanced

chromosomal translocations. A fusion gene can result from this translocation, which codes for a protein with an altered function. Here only one allele has to be affected to trigger malignant transformation (WS Krug et al., 2005).

An example for the activation of a proto-oncogene will be given later in the chapter on chromosomal translocations.

1.2.2 Chromosomal alteration

Until now, more than 56,000 chromosomal alterations have been reported across all main cancer types (Mitelman Database of Chromosome Aberrations in Cancer, JD Rowley, 1999). However, there are a number of recurrent balanced chromosomal rearrangements, especially translocations. For some there is compelling evidence that they are strongly associated with distinct tumor entities. These aberrations occur more often in hematological disorders than in malignant solid tumors. In acute myeloid leukemia, for example, 1,785 balanced aberrations were identified, of which 267 are recurrent balanced abnormalities. Whereas in breast cancer, only 343 balanced abnormalities could be detected of which only 13 are recurrent (F Mitelman, 2007).

To date, in hematopoietic disorders, 264 fusion genes have been identified involving 238 different genes. This means that 75 % of all currently known gene fusions present in hematological malignancies (F Mitelman, 2007).

Chromosomal alterations can be found by standard cytogenetic techniques in at least 70 to 80 % of leukemia cases on diagnosis (T Burmeister, 2000). These cytogenetic analyses provide diagnostic as well as prognostic information. In this way, these techniques become increasingly important for the clinical management of patients with hematological malignancies (B Johansson, 2004; I Panagopoulos, 2006).

1.2.3 Chromosomal translocations

A chromosomal translocation is a chromosomal aberration and describes the rearrangement of parts of the genetic material between two or more non-

homologous chromosomes (M Nambiar, 2008). This process may be balanced or unbalanced. A translocation is referred to as balanced if the amount of DNA remains unchanged after the translocation. In unbalanced translocations, the amount of genetic material is altered. That means either fragments of the DNA are lost or extra DNA fragments are added during the translation process (PD Aplan, 2006).

Two main types of chromosomal translocation are known: reciprocal (non- Robertsonian) and Robertsonian translocations.

Chromosomal translocations are referred to as reciprocal when segments are exchanged between two non-homologous chromosomes. They are usually balanced.

Robertsonian translocation, named after WRB Robertson, describes the fusion of two acrocentric chromosomes near the centromere region. Usually the short arm of the chromosomes is lost in this chromosomal aberration. Often Chromosomes 13 and 14 are involved (Q Mu, 2010; M Nambiar, 2008).

There are two main consequences of chromosomal translocations:

1. A proto-oncogene can come under the influence of a different promoter or enhancer, which can lead to an altered expression of the oncogene.
2. Two genes can fuse so that a new gene is created with a modified function (TH Rabbitts, 1994).

For both mechanisms, it is important that the reading frame is preserved (T Burmeister, 2000).

1.2.3.1 Overexpression of an oncogene

Proto-oncogenes are genes with a crucial role in cell physiology, cell differentiation or regulation of cell growth. A proto-oncogene can be activated or deregulated by genetic alteration and change into a real oncogene, which may promote malignant growth and in this way can contribute to malignant transformation. A common mechanism is juxtapositioning the proto-oncogene with a different promoter or enhancer (T Burmeister, 2000). Often immunoglobulin (Ig) or T-cell receptor (TCR)

gene regions are involved in that kind of chromosomal change. These gene regions are the only ones that are rearranged regularly in germ line DNA. This process takes place to generate active antigen-receptor genes. However, occasionally errors occur and other genes get rearranged instead.

This mechanism was discovered for the first time in Burkitt's Lymphoma. To date, three translocations have been associated with this B-cell malignancy. With 90 % of the cases, translocation t(8;14)(q24;q32) is the most frequent. The result is the juxtaposition of *cMYC* on Chromosome 8 with the immunoglobulin heavy chain (IgH) locus on Chromosome 14 (TH Rabbitts, 1994). The translocation occurs in the switch region of the IgH constant chain gene segments (JL Hecht, 2000; M Nambiar, 2008). In this way, *cMYC* is relocated near the enhancer of *IgH*, which leads to an alteration of its expression. *cMYC* has an important role in cell proliferation, differentiation, apoptosis and metabolism (stem cell renewal). In this way, overexpression of *cMYC* would have a great impact on multiple cellular processes. This may ultimately contribute to the malignant transformation. Other translocations position *cMYC* close to immunoglobulin light chain (IgL) κ (t(2;8)(p11;q24)) or IgL λ (t(8;22)(q24;q11)) (TH Rabbitts, 1994, F Mitelman, 2007). These processes are presumably also linked to the switch of recombination of Ig genes. Thus these chromosomal changes do not explain the entire transformation. In addition, mutations in components of the *p53* pathway (e.g. *p53*, *p19*, *ATM*) have been reported in Burkitt's Lymphoma patients (M Nambiar, 2008; AR Ramiro, 2006). Another example of overexpression of an oncogene is the translocation t(14;18) in follicular lymphomas. This translocation relocates the *BCL2* gene in the direct neighborhood of the enhancer of *IgH* on Chromosome 14. This results in an overexpression of *BCL2*, which leads to higher cell survival due to the (unregulated) anti-apoptotic qualities of *BCL2*.

Both examples are illustrated in Figure 1.1 (M Nambiar, 2008).

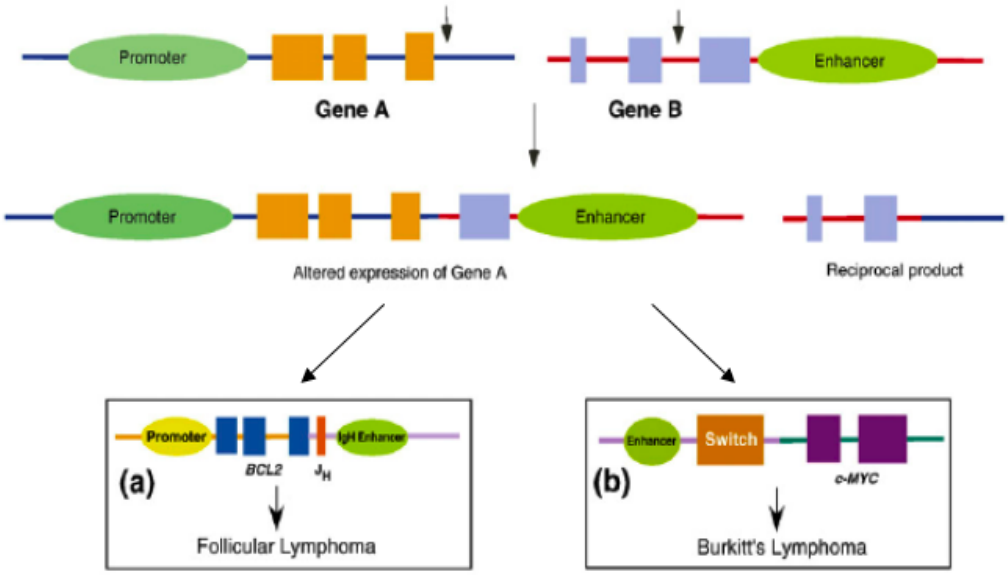

Figure 1.1: The figure illustrates one mechanism of how chromosomal translocation can contribute to malignant transformation. It displays the juxtaposition of the coding region of a proto-oncogene (gene A) with a promoter or enhancer of a different gene (gene B). This results in an altered expression of the oncogene and effects to the cell, depending on the function of the dysregulated gene. Two examples are shown in more detail: a) Follicular Lymphoma: The coding region of the *BCL2* gene (Chromosome 18) is relocated next to the enhancer of *IgH* (Chromosome 14). This enhances the anti-apoptotic functions of *BCL2* in the cell. b) Burkitt's Lymphoma: In the case of Burkitt's Lymphoma *cMYC* (Chromosome 8) is positioned next to the *IgH* enhancer by the translocation.

The lines represent double-stranded DNA, whereas the boxes represent exon regions. The black arrows in the first line indicate the breaking points. Adapted from M Nambiar, 2008.

1.2.3.2 Generation of a fusion gene

The other way in which a translocation can affect leukemogenesis is through chromosomal breaks within genes. Usually this happens in an intron region. If the reading frame is preserved, a chimeric fusion gene is generated (see Figure 1.2). The attributes of the chimeric genes can differ compared to the original function. The first cytogenetic abnormality that could be linked to cancer was the translocation t(9;22)(q34;q11) in chronic myeloid leukemia (CML) (A de Klein, 1982; JD Rowley, 1973). This translocation leads to a fusion of the *Abelson's tyrosine kinase* (*ABL*) gene on Chromosome 9q34 and the gene *"break point cluster region"* (*BCR*) on Chromosome 22q11. *ABL* codes, as the name indicates, for a tyrosine kinase, which shows, after its fusion with *BCR,* an increased activity (N Heisterkamp, 1985).

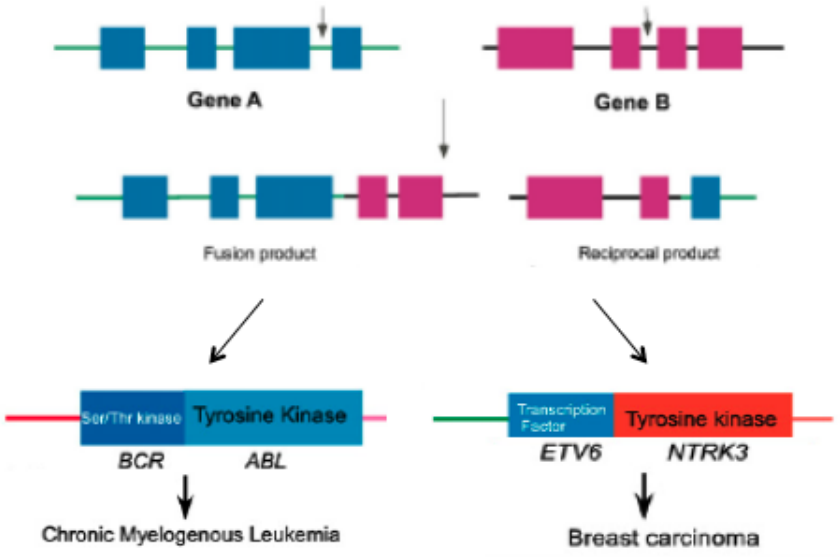

Figure 1.2: This figure demonstrates the generation of a fusion protein, also referred to as a chimeric gene, by chromosomal translocation. A chromosomal translocation can cause a fusion of the functional domains of e.g. gene A with a functional domain of gene B. The result is a new protein with altered or enhanced function. This new protein can, depending on the function, contribute to malignant transformation. Two examples are displayed above:

Left side: Chronic Mylogenous Leukemia: CML is characterized by a translocation involving Chromosomes 9 and 22. The affected genes are *ABL* on Chromosome 9 and *BCR* on Chromosome 22. The relevant gene fusion is located on Chromosome 22, which is commonly known as Philadelphia Chromosome. The resulting protein holds the tyrosine kinase of *ABL*. But due to the *BCR* part, the tyrosine kinase has a higher activity.

Right side: The figure depicts a common translocation in breast cancer. *NTRK3* is also a tyrosine kinase and is fused to *ETV6*, which is a transcription factor. The chimeric protein that is encoded by the fusion gene contributes to the tumor development.

The lines represent double-stranded DNA, whereas the boxes represent exon regions. The black arrows in the first line indicate the breaking points. Adapted from M Nambiar, 2008.

Also other fusion genes involved in malignant transformation contain tyrosine kinases. About 30 out of 90 protein tyrosine kinases can be connected with cancer (SD Turner, 2006). Depending on their alteration, timing or level of expression of the affected tyrosine kinases, they can directly or indirectly induce transforming events such as uncontrolled cell growth, genomic instability or protection of DNA-

damaged cells from apoptosis. Examples would be *NPM-ALK*, *TEL(ETV6)-JAK2* or *TEL-PDGFβR* (SK Bohlander, 2000).

1.3 ETV6

ETV6 (*ets variant gene 6*), which was formerly named *TEL* (*translocation ets leukemia gene*), is a member of a family of transcription factors known as the ets (erythroblast transformation specific) family. Most members of the ets family act as transcriptional activators. Only three members, namely *YAN*, *ERF* and *ETV6* show functions as repressors of transcription (AD Sharrocks, 2001).

ETV6 has highly conserved protein domain in common with other family members e.g. the ets domain or the HLH (helix loop helix) domain (T Oikawa, 2003; CM Slupsky, 1998; B Wasylyk, 1993). *ETV6*, however, is comprised of 652 amino acids and has two alternative variants of two alternative start codons at position 1 and at position 43 (SJ Grimshaw, 2004). The functional domains are depicted in Figure 1.3.

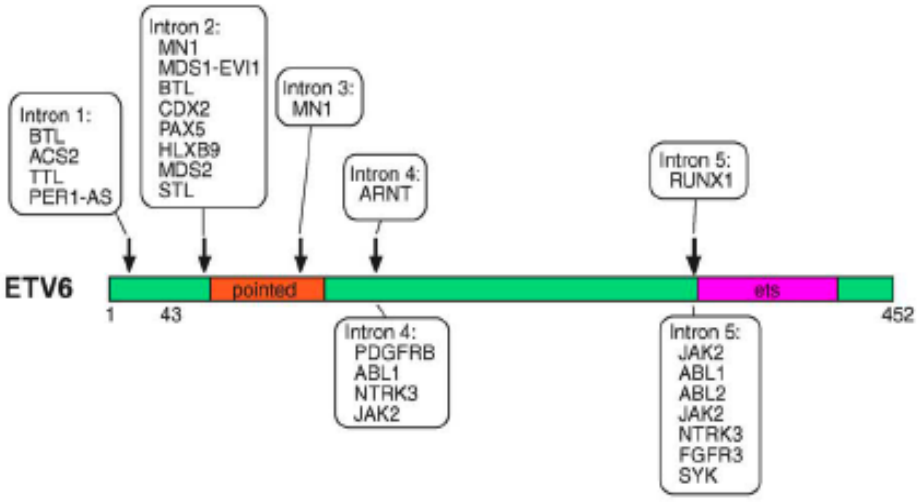

Figure 1.3: This figure depicts the functional domains of *ETV6*. The translocation breakpoints of diverse fusion partners are shown as well. Adapted from SK Bohlander, 2005.

1.3.1 *ETV6* function

ETV6 is widely expressed throughout the embryonic development in multiple organs. Although it was not possible to show a special role in embryonic hematopoiesis, there is a certain function of *ETV6* in vascular development (LC Wang 1997).

In adults as well, ETV6 shows a wide expression over different organs including hematopoietic cells (LC Wang 1998). Hock et al. established mouse models to determine the further tasks of *ETV6* in hematopoietic cells. They found that hematopoiesis is dependent on the expression of *ETV6*. Further they could show that hematopoietic stem cells (HSC) lacking *ETV6* have a limited clonal lifespan and therefore indicates that *ETV6* could have an important role in HSC survival. This would indirectly affect most hematopoietic cells, which are dependent on continuous regeneration due to their limited lifespan.

It was also shown that ETV6 has a great impact on the late development of the megakaryocyte lineage. ETV6 seems to act along with other transcript factors in this process (H Hock, 2004). Recent studies with transgenic mice models implied a distinct role of ETV6 is expanding erythroid precursors and the accumulation of hemoglobin (M Eguchi-Ishimae, 2009).

1.3.2 *ETV6* fusions

From the use of cytogenetic techniques, it is known that the short arm of Chromosome 12 is involved in multiple chromosomal rearrangements in different types of leukemia and myelodysplastic syndrome (H Kobayashi, 1994; MD Odero, 2001). *ETV6* is located on Chromosome 12p13 and is involved in more than 40 chromosomal translocations. Some fusion partners are very well known genes in leukemogenesis, such as *ABL1* and *RUNX1*. Others are not known and lack any obvious function (SK Bohlander, 2005).

Translocations in the *ETV6* region can be classified in three rough groups. One group contributes to leukemogenesis through activation of protein tyrosine kinases (PTK). The second group forms fusion genes of *ETV6* with transcription factors and other genes. The third group does not lead to a productive fusion protein and

therefore is presumably involved in the development of leukemia via overexpression of itself or neighboring genes. Certainly, this is only a vague summarization (see Figure 1.4). There are overlaps, such as translocations that show overexpression of a transcription factor. Those translocations would fit into group two and three (SK Bohlander, 2005).

1.3.2.1 Protein tyrosine kinases as fusion partners of *ETV6*

Fusions of *ETV6* with PTKs have been identified in different hematological (and non-hematological) malignancies, namely CMML, AML, early pre-B-ALL, T-ALL, atypic CML, myelodysplastic syndrome, peripheral T-ALL and some rare solid tumors. Fusion partners of *ETV6* that gain transformation potential through mechanisms such as constitutive activation of the PTK domain, autophosphorylation of the fusion protein or phosphorylation of other cellular proteins are *ABL1*, *ABL2*, *JAK1*, *NTRK3*, *FGFR3* and *SYK* (SK Bohlander, 2005).

The transformation potential of *ETV6/PTK* fusions is dependent on the presence and proper function of the pointed domain of *ETV6* and the PTK domain of the fusion partner. For example, for the fusion of *ETV6* with *PDGFR*β (platelet derived growth factor receptor β), it was shown that the *ETV6/PDGFR*β fusion seems to have transformation potency and to be critical for the development of chronic myelomonocytic leukemia (CMML) (TR Golub, 1994).

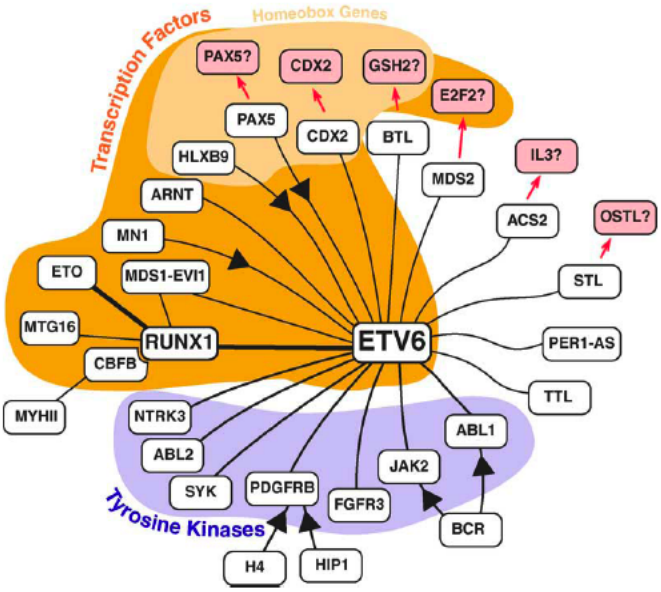

Figure 1.4: This figure depicts the translocation partner of *ETV6*. The colored fields mark the groups of genes that share a certain function. A gene fusion is indicated through a connecting line. Arrows point out that the N-terminal part of the fusion gene is more centrally located. Red arrows indicate transcriptional upregulation. Question marks designate that relevance is not yet proven. Adapted from SK Bohlander, 2005.

1.3.2.2 Transcription factors as fusion partner of *ETV6*

In different hematopoietic malignancies, fusion genes of *ETV6* with transcription factor have been described. The most common translocation involves *RUNX1* (*AML1*) and occurs in approximately 25 % of all childhood B-cell ALL cases (SA Shurtleff, 1995). The translocation t(12;21)(p13;q22) shows a more complex rearrangement that also includes material from Chromosome 1 (SK Bohlander, 2005; TR Golub, 1994). The fusion protein of ETV6 and RUNX1 consists of the pointed and central domain of ETV6 and the binding specific side of RUNX1. That means that the fusion protein can still bind the usual targets of RUNX1. Only, instead of transcriptional activation of its target genes, ETV6/RUNX1 shows repressive activity. This is mediated through the SAM and the central domain of ETV6 (R Fenrick, 1999; SW Hiebert, 1996).

Another example of a fusion of *ETV6* with a transcription factor is the fusion with *MN1*, which is only observed in some patients with AML or Myelodysplastic Syndrome (MDS). The MN1/ETV6 fusion protein presumably has transformation activity and interacts with transcriptional co-activators, p160 and p300 (A Buijs, 2000; KH van Wely, 2003). Later it was shown by the same group, that MN1/TEL

represses RAR (retinoid acid receptor)-RXR. This action is mediated through the dysfunction of a transactivation domain (KH van Wely, 2007).

The fusion *HLXB9/ETV6* has only been described in two cases of childhood AML, although the t(7;12)(q36;p13) occurs in about 20 % of childhood AML. The fusion protein probably deregulates the expression of *ETV6* target genes in early hematopoietic cells (HB Beverloo, 2001).

1.3.2.3 *ETV6* rearrangements leading to ectopic or aberrant expression

There are a number of translocations involving *ETV6* that play a role in leukemogenesis, presumably due to overexpression of one of the fusion genes or neighboring genes. Most of these fusions have only been shown in rare cases, mostly in acute leukemia. For example, the translocation t(12;13)(p13;q12) was detected in some cases of AML. It leads to a fusion of *ETV6* with the homeobox related gene *CDX2* (A Case, 1999), only, no fusion protein was found. Instead, *CDX2* itself was highly overexpressed. Later it was proven in a murine bone marrow model that this overexpression is the important factor for leukemogenesis (VPS Rawat, 2004).

For *BLT* (Brx-like translocated in leukemia) it was shown that rather the ectopic expression of *GSH2* than one of the two fusion proteins has a crucial part in the development of AML (J Cools, 1999; 2002).

However, there are also translocations involving *ETV6* and previously not identified genes. Examples of these genes would be *MDS2* and *STL*. The fusion of *ETV6* with *MDS2* was detected in one case of Myelodysplastic Syndrome, whereas *STL* was identified in one case of pre B-ALL. Both fusions code for very small proteins with no detectable function. This suggests that upregulation of neighboring genes is the main pathogenic mechanism. Possible affected genes could be *ID3*, *E2F2* or *RPL11* in the case of the translocation involving *ETV6* and *MDS2* and *OSTL* in the case of the fusion of *ETV6* with *STL* (SK Bohlander, 2005).

1.4 Translocation t(6;12)(q23;p13)

t(6;12)(q23;p13) is one of the translocations that involves *ETV6* and a previously unknown gene. The fusion partner was named *STL* (six twelve leukemia) gene by Suto et al. in 1997. The translocation t(6;12)(q23;p13) was first discovered in a precursor B-cell ALL cell line (SUB-B2), which was established from the leukemic cells of a 5-year-old boy with common ALL (LQ Zhang, 1993). To date, this translocation is unique. But two cases exist with the similar breakpoint t(6;12)(q21;p13) discovered in children with pre-B ALL (Y Hayashi, 1990). Fluorescence in situ hybridization (FISH) analysis with specific probes for 12p was necessary to discover t(6;12)(q23;p13) in the SUB-B2 cell line. Still it is possible that these cases are not really different from the cases with t(6;12)(q21;p13) discovered by Hayashi et al.

As *ETV6* translocations often show an open reading frame (ORF), it was the first hypothesis that a new fusion gene had been discovered with this translocation. But an ORF could not be identified either in the *ETV6/STL* fusion or in the reverse fusion. *ETV6/STL* only codes for a very small protein, which lacks any function (see Figure 1.5) (Y Suto, 1997).

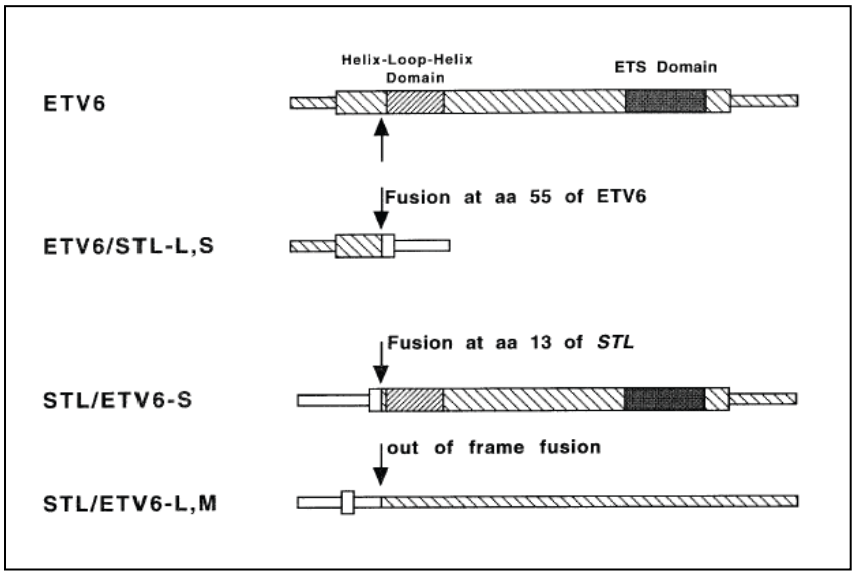

Figure 1.5: This figure depicts a diagram of the ETV6, ETV6/STL, and STL/ETV6 proteins. Adapted from Suto, 1997.

Because the fusion proteins did not seem to have any impact on the malignant transformation or any other detectable function, another previously unknown gene came into the focus of interest, because of its direct proximity to the translocation.

1.5 *OSTL* (opposite *STL*)

The newly discovered gene shares the first exon with *STL* but is transcribed in the reverse direction. This led to the name “opposite *STL*” (*OSTL*). It is localized at the band q23 in the chromosome 6. In human genome *OSTL* encodes for a protein with 275 aa, whereas the mouse protein consists of 307 aa. The mouse OSTL protein is 98 % identical to the human OSTL protein and puffer fish (*Fugu rubripes*) OSTL protein and human OSTL protein show a homology of 68 % (L Fontanari Krause, 2006).

The *OSTL* gene, respectively the encoded protein, were characterized in detail by Fontanari Krause et al. The OSTL protein is mainly located in the cytoplasm of mouse fibroblast cell lines. The protein does not show very high expression either in human or in mouse tissue. *OSTL* expression could be observed in skeletal, muscle, heart, testis, ovary, placenta, prostate and pancreas in human multiple Northern blots. In mouse Northern blots, it was only expressed in testis, ovary and liver. Northern blots were also performed with human leukemic cell lines, but only three EBV transformed lymphoblastoid cell lines (LCL B, D and R) and one transformed B-NHL cell line (Karpas422). Reverse trascription PCR experiments revealed expression of *OSTL* in naïve memory B-cells and plasma cells. This could indicate a particular role of *OST*L in B-cell maturation. Using whole mount in situ hybridization experiments on mouse embryos, Fontanari Krause et al. were able to detect *OSTL* in somites (myotome), first and second branchial arches, optic and otic vesicles, in the hair follicles of the vibrissae, and limb buds in mouse embryos examined from days 9.5 to 14.5. This could indicate that *OSTL* also has a particular role in the embryonic development of these structures.

Although there were several different splicing variants of *OSTL* detectable, only about seven seem to code for a long protein with functional domains. In fact the protein *OSTL* codes for, carries three functional domains: a N-terminal variant

RING (really interesting new gene) finger, a C-terminal RING finger and an In-between-RING-finger (IBR) domain. These domains show homologies to other human genes, *C. elegans, D. melanogaster* and *S. cerevisae*. This implies a high conservation in evolution.

The RING motive can be found in more than 400 proteins. They present with many different functions. A certain group of proteins can be summarized under the name RING-IBR-RING/TRIAD. This protein family is known to have the function as E3 ubiquitin ligase (AD Capili, 2004). This motive equals the structure of the OSTL protein.

The proteins HAX-1 and SIVA could be identified as interaction partners of OSTL by a yeast two-hybrid assay and confirmed by a co-immunoprecipitation assay. Both proteins are involved in B-cell survival and B-cell receptor signaling, although in opposite ways.

As the functional structure of OSTL equals the RING-IBR-RING/TRIAD, OSTL was tested whether it also shows ubiquitin ligase activity. If this is the case, HAX-1 and SIVA are not substrates. Both show no ubitiquination in an ubiquitination assay (L Fontanari Krause, 2006).

1.6 Aim of this work

Our main interest in this work was to receive more information about the *OSTL* in the context of leukemia. Especially we were interested in how *OSTL* is expressed in different types of leukemia. This way we hoped to find a correlation between the overexpression of *OSTL* and a certain leukemia subtype.

Therefore we performed Microarray analysis of 129 leukemia patients for a rough overview of the expression levels of *OSTL*. Then we validated these results using real-time PCR. For this study, we included 40 patients with acute leukemia or chronic myeloid leukemia.

2 Material and Methods

2.1 Material

2.1.1 Chemicals, kits and materials

Material	Company
1-kb-DNA molecular weight marker	Life Technologies, Eggenstein, Germany
1.5 ml micro centrifuge tube	Eppendorf, Hamburg, Germany
15 ml polypropylene conical tubes	Becton Dickinson, Meylan, France
50 ml polypropylene conical tubes	Becton Dickinson, Meylan, France
Acetic acid	Merck, Darmstadt, Germany
Agarose	ICN Biomedicals Inc.
Ampicillin	Pan Biotech, Aidenbach, Germany
Aqua bidest.	Millipore, Eschborn, Germany
Boric acid	Carl Roth, Karlsruhe, Germany
Bovine serum albumin	Life Technologies, Eggenstein, Germany
Cell culture medium DMEM	Pan Biotech, Aidenbach, Germany
Cell culture medium RPMI	Pan Biotech, Aidenbach, Germany
Chloroform	Sigma, Deisenhofen, Germany
Deoxyribonuclease I, Amplification Grade	Life Technologies, Eggenstein, Germany
DEPC	Carl Roth, Karlsruhe, Germany
DMSO	Sigma, Deisenhofen, Germany
DNA polymerases	Fermentas GmbH, St. Leon-Rot, Germany
dNTP Set, PCR Grade	Life Technologies, Eggenstein, Germany
EDTA	Carl Roth, Karlsruhe, Germany
Electroporation cuvettes	PeqLab, Erlangen, Germany
Eppendorf tubes	Eppendorf, Germany
Ethanol	Merck, Darmstadt, Germany
Ethidium bromide	Carl Roth, Karlsruhe, Germany

Fetal Bovine Serum	Gibco, Life Technologies, Paisley, Scotland
Beveled Filter Tips (different sizes)	Starlab GmbH, Ahrensburg, Germany
Isopropanol	Carl Roth, Karlsruhe, Germany
MicroAmp® Fast Optical 96-Well Reaction Plate with Barcode, 0.1 ml	Applied Biosystems, Foster City, USA
MicroAmp® Optical Adhesive Film	Applied Biosystems, Foster City, USA
O'Range Ruler, 50bp DNA Ladder	Fermentas GmbH, St. Leon-Rot, Germany
PBS	Pan Biotech, Aidenbach, Germany
Penicillin/Streptomycin	Pan Biotech, Aidenbach, Germany
Pipette tips	Carl Roth, Karlsruhe, Germany
Plastic material for cell culture	Greiner Labortechnik, Frickenhausen, Germany Sarstedt, Nümbrecht, Germany Corning, USA
RNase Away	Carl Roth, Karlsruhe, Germany
ThermoPol Reaction Buffer	New England Biolabs GmbH
Thermoscript RT-PCR System	Life Technologies, Eggenstein, Germany
Tris	Carl Roth, Karlsruhe, Germany
Trypan blue	Life Technologies, Eggenstein, Germany
Trizol	Life Technologies, Eggenstein, Germany

2.1.2 Equipment

7900HT Fast Real-Time PCR System with Fast 96-Well Block Module (Applied Biosystems, USA)

Centrifuge 5417 R (Eppendorf, Germany)

Centrifuge 5417 C (Eppendorf, Germany)

Cytospin (Cytospin 2 Shandon, USA)

Gel Electrophoresis System (Labortechnik GmbH, Germany)

GeneAmp PCR System 2400 and 9700 (Applied Biosystems, USA)

Microscope (Zeiss Axiovert 200 M, Zeiss Axiovert 135, Germany)

Nano Drop (Thermo Fisher Scientific Inc., USA)

Pipetman-Pipetts (Gilson Inc., USA)

UV Spectrophotometer (Pharmacia Biotech, Germany)

2.1.3 Buffer and solutions

DEPC treated water

Diethylpyrocarbonate was added to bi-distilled water to reach a 0.1% solution. The mix was then stirred with a stir bar over night at room temperature and on the next day autoclaved for 30 min.

EDTA (ethylene diamine tetraacetic acid)

For 500 ml stock solution of 0.5 M EDTA (pH 8.0), 93.05 g EDTA disodium salt was dissolved in 400 ml deionized water. To achieve a complete solution of EDTA disodium salt, the pH had to be adjusted to 8.0. This was achieved by adding NaOH under continuous stirring until the desired pH was reached. Once the pH was adjusted, the volume of the solution was adjusted with deionized water to the total volume of 500 ml and autoclaved.

TBE-Electrophoresis Buffer

To prepare 1 liter of 10 x TBE buffer, as stock solution, 108 g Tris base, 55 g Boric acid and 40 ml 0.5 M EDTA (pH 8.0) were transferred into a 1 l glass flask. Then bidest. water had to be added to adjust the solution to a total volume of 1 l. The contents were then stirred with a stir bar until all the ingredients had dissolved.

The buffer was stored at room temperature and discarded if a precipitate formed.

For agarose gel electrophoresis, a 1:10 dilution was prepared to achieve 1 x TBE Buffer.

2.1.4 Cell lines

DG-75:

Cell type: Human Burkitt's Lymphoma cells

This cell line was established from the pleural effusion of a 10-year-old boy with refractory Burkitt's Lymphoma in 1975.

(Provided by Medhani Mulaw Ph.D., Helmholtz Zentrum, Munich)

Ben-Bassat et al., Int J Cancer (1977)

LCL B:

Cell type: Lymphoblastoid transformed cell

(provided by Dr. Luciana Fontanari Krause, Helmholtz Zentrum, Munich)

SEM:

Cell type: Precursor B cell of type B-I

The cell line was established from the peripheral blood of a 5-year-old girl at relapse of acute lymphoblastic leukemia (ALL) in 1990. The girl was reported to carry the t(4;11) *MLL-AF4* translocation.

(provided by Dr. Luciana Fontanari Krause, Helmholtz Zentrum, Grosshadern, Munich)

Greil et al., Br J Haematol (1994)

Marschalek et al., Br J Haematol (1995)

2.1.5 Media

DMSO freezing medium

Cells were frozen in filter-sterilized and heat-inactivated FCS with 10 % DMSO.

Cell culture medium

To complete the RPMI and DMEM media, 10 % fetal calf serum (heat-inactivated) and 1 % Penicillin/Streptomycin solution (10.000 U/ml Penicillin, 10 ng/ml Streptomycin) were added to RPMI or DMEM medium to achieve a total volume of 500 ml.

Dulbecco´s Modified Eagle medium (DMEM)

4.5 g/l Glucose

0.5 g/l L-Glutamine

0.1 g/l Sodium Pyruvate

3.7 g $NaHCO_3$

Sterile filtered

Penicillin/Streptomycin solution

10,000 U/ml penicillin

10 mg/ml streptomycin

Roswell Park Memorial Institute culture medium (RPMI 1640)

0.02 g/l L-Glutamine

2.0 g/l $NaHCO_3$

Sterile filtered

2.1.6 Patients

The Laboratory for Leukemia Diagnostics, Department of Medicine III, Klinikum Grosshadern, provided cDNA samples from anonymous leukemia patients.

The study includes 10 patients with CML, 10 AML patients with normal karyotype (AML,nk) and 20 ALL patients from 4 different subgroups (5 samples of ALL, Philadelphia Chromosome positive (ALL-Ph+); 5 patients with the translocation t(4;11); 5 patients with common ALL and 5 patients with T-cell ALL).

The table displaying the individual patients included in the relative quantification experiments can be found in the Appendix. It shows the type of leukemia, age at diagnosis, karyotype and molecular marker of each patient.

Sample 12 (ALL-Ph+) could not be included because of too little cDNA material.

2.1.7 Plasmids

pGBKT7/OSTL maxi

pGBKT7/OSTL midi

pGBT9/E06 mini

pMIG/OSTL maxi

The plasmids were prepared and provided by Dr. Luciana Fontanari Krause, Helmholtz Zentrum, Munich, Germany. They were used for primer testing and optimization before they were used for real-time PCR. In real-time PCR experiments the plasmids were used as positive control.

2.1.8 Primers and probes

Oligonucleotides used for DNA amplification and real-time PCR were designed using the MacVector 7.0 software program as well as Primer Express and were purchased from Metabion GmbH (Martinsried, Munich). The sequences of the primers and probes are listed in Table 2.1. As endogenous controls, we used standardized ready-made primer and probe sets provided by Applied Biosystems, USA (see Table 2.2).

The fluorogenic probes are specifically designed for each primer pair. The 5'-end of the oligonucleotide probes are labeled with a fluorescent reporter dye. For this, we used FAM dye. On the 3'-end a quencher is bound, which reduces the fluorescence emitted by the reporter dye, while the probe is intact. As quencher we used BHQ-1.

Oligoname	Sequence	Exon
hTBP-F	5’-GCACAGGAGCCAAGAGTGAA-3’	Exon 5/6
hTBP-R	5’-GTCTGAGTGTGGCAGGGACTC-3’	Exon 6
hGAPDHT	5’-GCACCACCAACTGCTTAGCACC-3’	Exon 7
hGAPDHB	5’-GTCTGAGTGTGGCAGGGACTC-3’	Exon 9
E06OSTL601T	5’-AGAGGAATGCCCAGAAGTGTCC-3’	Exon 3
E06OSTL761B	5’-ACTGAGGTTTGATGTGTGGTCTCC-3’	Exon 4
E06OSTL196T	5’-TGTGCGAGGAGTGCCTCAAAG-3’	Exon 1d
E06OSTL381B	5’-TGGTGCTGGAATCAATACGGC-3’	Exon 2
E06OSTL374T	5’-CAGCACCAAGCCATGTCCTC-3’	Exon 2
E06OSTL501B	5’-AACACCAGACGAATTGGCAGG-3’	Exon 3
E06OSTL734B	5’-AAATCGGAGCTGGCGGTATC-3’	Exon 4
OSTL-436/536FW	5'-CCCTTCCAGATCAGAAAGCAAA-3'	Exon 2/3
OSTL-436/536RV	5'-TGCAGTTAACACCTTCATTCCAA-3'	Exon 2/3
OSTL-436/536Probe	5'-ACAAAATCCAGTGCCCTACCTGCCAATTC-3'	Exon 2/3
OSTL-574/647FW	5'-GGCCAGCGAAATTGAGCAT-3'	Exon 3/4
OSTL-574/647RV	5'-CAGTTCGCTGGATGTGGATCT-3'	Exon 3/4
OSTL-574/647Probe	5'-AGGAATGCCCAGAAGTGTCCAAAGTGC-3'	Exon 3/4
OSTL-783/883FW	5'-TCCCAGAGAGACCTCATTTAAGGA-3'	Exon 4/5
OSTL-783/883RV	5'-CCCTAGTGCCAATCCCAAAA-3'	Exon 4/5
OSTL-783/883Probe	5'-CGAGGGTCAGTCTGTGCTGGAAAATT ATTCAT-3'	Exon 4/5
OSTL-861/961FW	5'-TGGTTTTGGGATTGGCACTAG-3'	Exon 5/6
OSTL-861/961RV	5'-TGTCCGTGATCGTTTTCTCTGT-3'	Exon 5/6
OSTL-861/961Probe	5'-CGGTTGTAATCGGTTTATTTGTATTTCCTAT CTATTGCCT-3'	Exon 5/6

Table 2.1: This table displays the names of the primers used in this study, the corresponding sequence and the Exon, where the primers bind.

Endogenous Controls
Human ACTB (beta actin) Endogenous Control (VIC / TAMRA Probe, Primer Limited)
Human GAPD (GAPDH) Endogenous Control (FAM™ Dye / MGB Probe, Non-Primer Limited)
Human TBP (TATA-box binding protein) Endogenous Control (VIC / MGB Probe, Primer Limited)

Table 2.2: This table gives details to the endogenous controls used for real-time PCR.

2.1.9 Software

- Microsoft Excel 2011 for Mac, version 14.1.0
- Microsoft Excel 2011 for Mac, version 14.1.0
- Microsoft Power Point 2011 for Mac, version 14.1.0
- Microsoft Word 2011 for Mac, version 14.1.0

  → For data analysis, text editing and figure management
- Primer Express® software v3.0

  → For primer design
- RQ Manager 1.2

  → For data analysis of the relative quantification experiments
- SDS software

  → Using TaqMan 7500H, set up and data generating for absolute quantification experiments

2.1.10 Internet search

- BLAST search (Basic Local Alignment Search Tool) for DNA or protein sequence homology search
  → http://blast.ncbi.nlm.nih.gov/Blast.cgi
- DSMZ German Collection of Microorganisms and Cell Cultures (Deutsche Sammlung von Mikroorganismen und Zellkulturen GmbH) for Information about cell lines
  → http://www.dsmz.de/
- PubMed for Scientific Literature
  → http://www.ncbi.nlm.nih.gov/pubmed/
- Genome Browser for validating DNA sequences
  → http://genome.ucsc.edu/

2.2 Methods

2.2.1 Cell culture

To ensure sterile conditions required for mammalian cell culture, all procedures were carried out in a vertical laminar-flow hood (BDK Luft- und Reinraumtechnik GmbH). The cells of the cell lines (see chapter 2.1.4) were grown in commercially available cell culture flasks and incubated at 37°C in a humid atmosphere containing 5 % CO_2. All materials used in the laminar-flow hood were sterilized by treating the surface with 70% ethanol or UV light for 15 min. For suspension cells, commercially available DMEM and RPMI were used that we supplemented with 10% FCS and antibiotics (100 U penicillin and 100 ng streptomycin/ml). The cells were split according to the cell growth rate and density. For cryopreservation of a cell line ~$6x10^6$-$1x10^7$ vital cells in a logarithmic growth phase were suspended in 1.5 ml FCS with 10 % DMSO in 1.8 ml in a 1.8 ml cryotube. Before being stored permanently in liquid nitrogen, the tubes were placed in a -80°C freezer for 24 hours.

2.2.2 RNA Isolation with Trizol reagent

The RNA Isolation from suspension cells was performed using Trizol Reagent following the manufacturer's instructions.

The cells were suspended briefly and then counted. 5-10 x 10^6 cells were selected and centrifuged at 1000 rpm for 5 min to pellet the cells. The medium was discarded and 1 ml of Trizol Reagent was added and homogenized through repetitive pipetting. After incubating for 5 min at 15 to 30°C, 0.2 ml of chloroform was added and the tube shaken vigorously for 15 sec. During centrifuging at 12,000 x g for 15 min, the sample was separated into three phases: a lower red phenol-chloroform phase, a whitish interphase containing DNA and an upper colorless, aqueous phase containing RNA. The aqueous phase was transferred to a new sterile tube. To precipitate RNA, 0.5 ml isopropyl alcohol was added and incubated for 10 min. After another centrifugation at 12,000 x g the RNA was visible as a pellet. The supernatant could be removed and the pellet washed by adding 1 ml 75 % ethanol and mixed by vortexing. Then the sample was centrifuged at 7,500 x g for 5 min, the ethanol discarded and the RNA pellet air-dried for 5 to 10 min. Afterwards, the RNA was dissolved in RNase free water through pipetting and the sample incubated for 10 min at 55 to 60°C. The RNA was then stored at -80°C.

Centrifugation was performed at a temperature of 2 to 8°C and incubation steps at 15 to 30°C.

To determine the quality and yield, the RNA was measured in a UV spectrophotometer (Pharmacia Biotech) at the wavelengths of 260 and 280 nm, normally diluted 2 µl in 198 µl sterile bidest. water. Each sample was measured twice and only accepted if within the linear range of 4 µl/ml to 40 µl/ml.

The quality was tested with Agarose Gel Electrophoresis. A diluted aliquot was run on 1,5 % Gel stained with ethidium bromide.

2.2.3 Deoxyribonuclease I treatment

All RNA used for reverse transcription PCR (cDNA synthesis) was treated with Deoxyribonuclease I to increase the purity of the RNA sample. The DNase used was included in a kit by Invitrogen. It was purified from bovine pancreas and had a specific activity of ≥ 10,000 U/mg. Four tubes were prepared, two with and two without Deoxyribonuclease. In the negative samples, the Deoxyribonuclease was replaced by Rnase-free water. In a Rnase-free Eppendorf tube 1 μg RNA dissolved in DEPC water was mixed with 1 μl 10 x DNase I Reaction Buffer and 1 μl DNase I (Amp Grade, 1 U/μl). To the reaction mix, DEPC water was added to reach 10 μl total mix. The tubes were then incubated for 15 min at room temperature. To inactivate Dnase, I 1 μl of 25 mM EDTA was added and afterwards heated to 65°C for 10 min. Immediately after this procedure, reverse transcription PCR was performed.

2.2.4 Microarray analysis

For the microarray analysis bone marrow samples of 139 patients were included. 129 patients were diagnosed with leukemia and 10 showed no signs of disease (normal bone marrow). The cohort included 13 leukemia subgroups, namely CML (chronic myeloid leukemia), *CALM/AF10* positive leukemia, 7 AML subtypes (AML_nk with normal karyotype; AML_MLL with *MLL* rearrangement; AML_M4 with *CBFB/MYH11* fusion; AML_M3 with *PML/RARA* fusion; AML_M2 with *AML1/ETO*; AML_FLT3 with *FLT3* mutation; AML_comp with complex aberrant karyotype), and 4 ALL subtypes (ALL_Ph+ with *BCR/ABL* fusion, ALL_MLL with *MLL* rearrangements, ALL_BA (pre B-cell ALL), ALL (common ALL)).

A microarray chip contains a glass slide on which abundant DNA fragments of certain regions are attached in so called spots. The cDNA or RNA samples are labeled with a specific fluorescent dye. The samples will hybridize to the DNA at the spots. After hybridization a laser can detect the fluorescence emitted by the probes. The emitted fluorescence is proportional to the amount of RNA/cDNA added (M Babu, 2004).

For this analysis total mRNA obtained from the 139 bone marrow samples was used. The samples were processed and analysed on the Affymetrix HG-U133A and HG-U133B chips as described by Schoch et al in 2002. Normalization of the data set was performed using VSN (Variance stabilization and calibration for microarray data) (W Huber, 2002). The expression levels were depicted in a box plot generated in the “box plot function”. The expression signal intensities are shown on a logarithmic scale.

2.2.5 Agarose gel electrophoresis

For analyzing the RNA yield and PCR products, agarose gel electrophoresis was performed. Although the expected PCR were quite small, between 100 and 150 bp, usually 1.5% agarose gels were prepared. Therefore 0.75 g agarose was heated with 50 ml 1 x TBE Buffer until boiling to dissolve the agerose entirely. After 5 min cooling down, ethidium bromide was added to reach a final concentration of 0.5 µg/ml. DNA and RNA were prepared with 1-2 µl DNA Loading Buffer (10 x) with a higher density than the buffer, to let the sample sink into the pockets and visualize the progress on the gel while running. Depending on the size of the expected DNA fragment, an appropriate molecular weight marker was used (e.g. 50 bp DNA Ladder by Fermentas). The gel then was run between 60-100 V. The DNA was visualized under UV light (365 nm).

2.2.6 cDNA synthesis (reverse transcription PCR)

For the purpose of testing the primers under more comparable conditions to patient samples, reverse transcription PCR was performed on several cell lines for cDNA synthesis. The Thermoskript reverse transcription PCR System by Invitrogen was used. All steps were performed according to the manufacturer’s suggestions. Before starting, the bench space and the material used were cleaned with “RNase away” to prevent RNase contamination. As primer, we chose Random-Hexameter for the cDNA synthesis. Always approximately 1 µg RNA was used per reaction tube. We prepared four tubes per RNA sample, D+RT+, D+RT-, D-RT+ and D-RT- (D = DNase treatment, RT = cDNA synthesis, + = performed,

- = negative control). In this way, the procedure could be evaluated concerning its success.

In the first step, 9 µl of the DNase treated RNA samples were transferred into 0.5 µl reaction tubes and mixed with 1 µl Random-Hexameter and 2 µl of 10 mM dNTP mix per tube. This mixture was then incubated at 65°C for 5 min and thereafter placed on ice. This was performed to remove possibly formed secondary structures of the RNA to improve the cDNA synthesis. Then in each tube 4 µl of 5 x cDNA Synthesis Buffer, 1 µl of 0.1 M DTT, 1 µl RNaseOUT (40 U/µl), 1 µl DEPC water and 1 µl Thermoskript RT were added. According to the scheme above, in two tubes Thermoskript RT was replaced by DEPC water.

The tubes were then transferred to the thermal cycler where they were incubated at 25°C for 10 min, followed by 50 min at 50°C according to the protocol required for Random-Hexameter. The reaction was terminated by heating the mix to 85°C for 5 min. To the now synthesized cDNA was added 1 µl RNase per reaction and then incubated for 20 min at 37°C.

The cDNA could then be stored at -20°.

The success of the synthesis was tested by PCR with GAPDH primers, using the protocol as follows: 95°C 2 min, then 30 cycles with 30 sec 95°C, 30 sec 60°C and 30 sec 72°C, followed once by 72°C for 5 min. Also the DNA quantity was measured using Nano Drop (Thermo Fisher Scientific Inc.). For this, a 1:10 dilution was prepared and vigorously suspended. From this dilution we measured a two-microliter drop three times. We obtained the following measurements: concentration in ng/µl, wavelength A260 and A280, as well as the ratios 260/280 and 260/230. Samples with an A260/A280 ratio between 1.8 and 2.2 were accepted.

2.2.7 Polymerase chain reaction

Polymerase chain reaction (PCR) is a commonly used technique for DNA amplification and is based on a repetition of cycles consisting of denaturation of double-stranded template (cDNA or Plasmid), primer annealing and synthesis of new DNA sequence with a heat-stable DNA polymerase (taq polymerase). An

initial step with a temperature of about 95°C is required for initial complete denaturation of the template, as well as finally a prolonged extension step to ensure that all single-stranded DNA fragments are fully extended.

The Platinum *Taq* DNA Polymerase (Invitrogen) was used according to the manufacturer's instructions. The PCR buffer contained an approved amount of magnesium.

First, a master mix was prepared using sterile tubes, pipettes, and pipette tips (sterilized in the UV Stratalinker) with all reagents on ice as described in the following paragraphs.

PCR mix per reaction:

Platinum *Taq* DNA Polymerase	0.13 µl
10 x PCR buffer	2.0 µl
dNTPs (2 mM)	2.0 µl
5' Primer (10 µM)	0.5 µl
3' Primer (10 µM)	0.5 µl
Bidest. water	up to 19 µl

19 µl of the reagent mix was pipetted into thin-wall PCR tubes (0.2 ml), 1 µl of template DNA (~100 ng) was added in each tube and the sample was placed immediately in the thermocycler GenAmp PCR System 2400 and 9700. (Applied Biosystems).

The conditions for the PCR were programmed as shown below:

1.	95°C	2 min	initial denaturation

followed by 20-30 cycles of step 2 - 4:

2.	94°C	30 sec	denaturation
3.	55-60°C (primer dependent)	30 sec - 1 min	annealing
4.	72°C (template dependent)	1 min	elongation
5.	72°C	5 min	finish elongation
6.	4°C	∞	reaction end

The tubes could then be stored at 4°C.

The result of the PCR was tested with Agarose Gel Electrophoresis using a 0.5 to 1.5 % gel depending on the size of the expected DNA fragment.

2.2.8 Real-time PCR (quantitative PCR)

Real-time PCR also known as quantitative PCR (q-PCR) is a modified system based on the traditional polymerase chain reaction that uses fluorogenic probes to observe the process of the reaction in real time. This method allows quantifying a certain DNA fragment absolutely and relatively. There are basically two systems in real-time PCR, SYBR Green, a dye that detects all double-stranded DNA and the TaqMan Probe System, where the probes only bind a specific sequence.

For this work, we decided to use the TaqMan system. The specific primer and probe sets were designed using Primer Express Software (Applied Biosystems) and endogenous control gene sets that were predesigned and provided by Applied Biosystems. All reagents and samples used were kept on ice for the whole duration of working with them. Only sterile tubes, pipettes as well as filtered pipette

tips were used. For each sample, triplicates were prepared to increase the validity of the experiment.

General preparations:

A master mix was prepared for each primer and probe set used in the run. For the endogenous controls, 1 µl primer/probe mix was added to 10 µl Universal PCR Master Mix (2 x). For the self-designed primer/probes, the mix was prepared as follows:

PCR-Mix per reaction:

10 µl TaqMan Universal PCR Master Mix (2 x)
1.5 µl primer forward (10 µM)
1.5 µl primer reverse (10 µM)
0.5 µl fluorogenic probe (10 µM)

11 µl of the endogenous control mix and 13.5 µl of the target gene mix were pipetted into the designated wells of the Fast Plate. After this, 0.1 µg to 100 µg cDNA diluted in 9 µl (endogenous controls) or in 6.5 µl (target gene probes) was also inserted into the designated wells so that the final volume was 20 µl per reaction. The plates were sealed with optical adhesive covers and then centrifuged briefly. The reaction mix had to be located at the bottom of the well and should not contain any bubbles.

The plate could then be placed in the 7500H TaqMan System. Further adjustments were done with the SDS software (Applied Biosystems), which is connected to the TaqMan System.

After choosing the plate size and the selected method, the detector had to be selected for each well.

Cycling Conditions

Initial steps:

2 min at 50°C	AmpEraseUNG® activation
10 min at 95°C	AmpliTaq Gold® DNA Polymerase activation

Cycling steps (40 to 45 repetitions):

15 sec at 95°C	melting double-stranded DNA
1 min at 60°C	annealing and extending

2.2.8.1 Absolute quantification

In the case of Absolute quantification, a series of 10-fold dilutions was prepared from the target as well as from the standard. For the standard, plasmids (see chapter 2.1.7) in known quantities were used. This task of the sample has to be chosen in the SDS software: “unknown”, “no template control” and “standard”. Finally, the quantity has to be entered into the system.

The results were presented in the SDS software and shown in standard curves based on the C_t-values or could be exported as raw data for further use.

2.2.8.2 Relative quantification

To prepare for this method, target genes (the genes of interest) and endogenous control genes (constantly expressed housekeeping genes for the use of normalization) have to be chosen. This task has to be selected in the SDS software.

The results data can be viewed and adjusted with RQ Manager software (Applied Biosystems). The data can be exported in graphic illustration as well as a raw data set.

3 Results

3.1 Microarray analysis

To receive a first picture of the expression profile of the *OSTL* gene we were able to use data of existing microarray analyses. The differential expression data of *OSTL* was extracted and a box plot was generated using this data (see Figure 3.1). The microarray analysis included 129 patients suffering from 13 different leukemia types, and 10 normal bone marrow samples. The cohort was composed of patients with chronic myeloid leukemia (CML), seven different acute myeloid leukemia (AML) subtypes and four subgroups of acute lymphatic leukemia (ALL).

OSTL shows the highest expression in CML and the lowest expression in the ALL subgroups as well as in patients with the CALM/AF10 translocation. The expression of *OSTL* was approximately twice as high in CML compared to AML.

The data acquired by microarray only represents a trend of the expression. So we decided on a real-time PCR analysis to confirm the results.

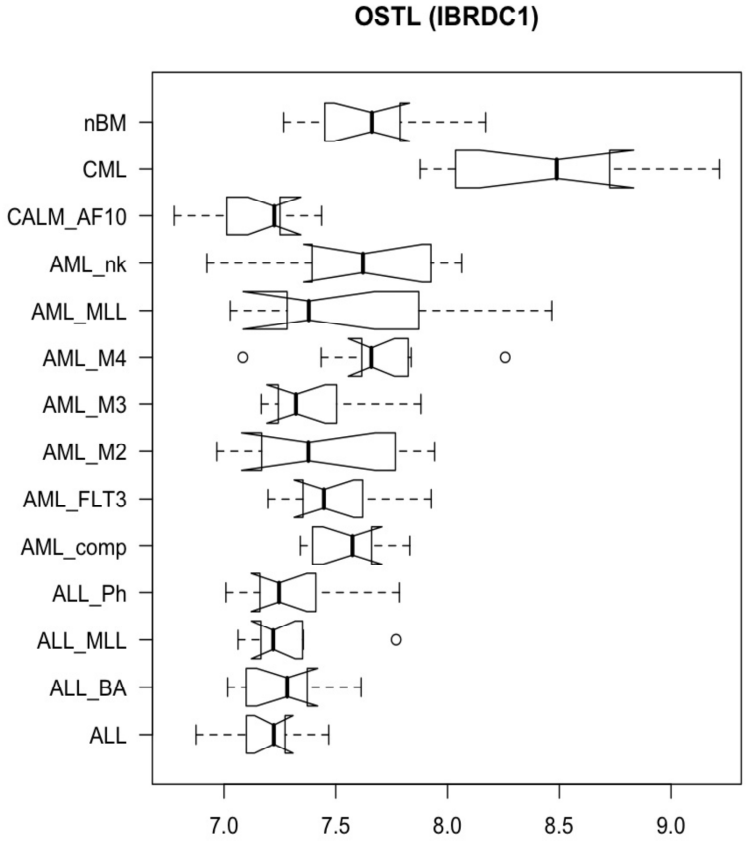

Figure 3.1: The plot in this figure displays the differential expression of *OSTL* in a cohort of 129 leukemia patients and 10 patients with no signs of disease. The box plot shows the expression levels of *OSTL* (IBRDC1) using mRNA samples of normal bone marrow (nBM), CML (chronic myeloid leukemia), CALM/AF10 positive leukemia, 7 AML subtypes (AML_nk with normal karyotype; AML_MLL with MLL rearrangement; AML_M4 with CBFB/MYH11 fusion; AML_M3 with PML/RARA fusion; AML_M2 with AML1/ETO; AML_FLT3 with FLT3 mutation; AML_comp with complex aberrant karyotype), ALL_Ph+ with BCR/ABL fusion, ALL_MLL with MLL rearrangements, ALL_BA (pre B-cell ALL) and ALL (common ALL). The normalized and variance stabilized expression values are shown on a logarithmic scale (approximately log 2). Big bars represent median, boxes represent the 25-75% quantile range (inter quantile range: IQR) and whiskers represent the 1.5-fold IQR. Small cycles represent outliners. An expression value was considered as an outliner, if the value was more than 1.5 IQR below or above the first or third quantile, respectively.

The highest expression was found in the group of CML patients. Whereas by trend the groups with the lowest expression were the ALL samples as the CALM/AF10 samples.

3.2 Quantitative PCR experiments

In order to validate the expression levels of *OSTL* that we obtained in the microarray analysis, real-time PCR, also referred to as quantitative (q-) PCR, was used.

Real-time PCR can be performed in one step, where reverse transcription and the PCR reaction with fluorescence recording are done in one step. The patient samples were provided in cDNA. So we used two-step real-time PCR from the beginning.

To validate the real-time PCR assay we tested the primers and calculated their efficiency.

3.2.1 Establishment

3.2.1.1 SYBR Green system

The SYBR Green System is a widely used real-time PCR system. The SYBR Green I fluorescent dye binds all double-stranded DNA and then emits fluorescence. The intensity corresponds with the amount of dsDNA in the reaction. Specific design of fluorogenic probes is not necessary with this method. We designed the primer pairs following all the approved standards. Namely, we just selected primer with a length in a range of 18 to 22 bp. The GC percentage was between 40 % and 60 % and the melting temperature was selected to be not lower than 52°C and not higher than 58°C. We also avoided primer that would form secondary structures. For the SYBR Green system it is recommended to have short amplicon sizes. So the primer pairs were designed so that they were in the range of between 90 bp and 190 bp in length. All primers spanned an exon-exon junction to ensure only cDNA was detected. In the figure below, the location of the amplicons is displayed in a schematic presentation of the cDNA sequence of *OSTL*.

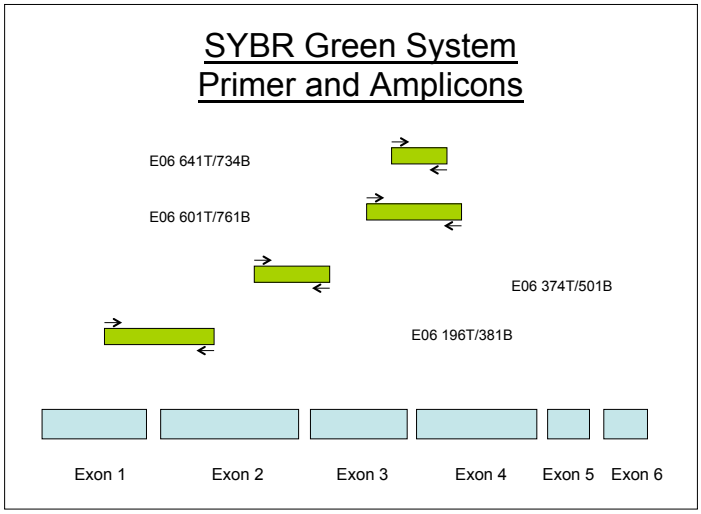

Figure 3.2: This figure depicts the location of the different amplicons in relation to the exons of *OSTL*. Amplicons are represented in green bars and primers as black arrows and the exons of *OSTL* are depicted as light blue bars in this figure.

We performed traditional PCR to examine the primer pairs. The Primers and corresponding amplicons are demonstrated in Figure 3.2. In this way we could adjust all parameters to the ideal working conditions for the real-time PCR. Thus we could expect an optimal performance of the reaction in real-time PCR. First we tested the primers in plasmids. For this purpose, we diluted all available plasmids with *OSTL* inserts. The plasmids were obtained from previous experiments (L Fontanari Krause). We used a final concentration of 10 ng/μl, which equals approximately 1 x 10^{10} molecules per microliter and performed PCR in the usual program with the appropriate annealing temperature for each primer pair. We added 1 μl of plasmid dilution per reaction. This means each reaction contained 10 x 10^{10} molecules that all held the target sequence. This high concentration provided an overflow of target. Under these conditions, most primers seemed to work well and produced the expected products. Only with E06-641T/734B additional bands appeared. They might have been caused by splice variants that are known for the location of the amplicon.

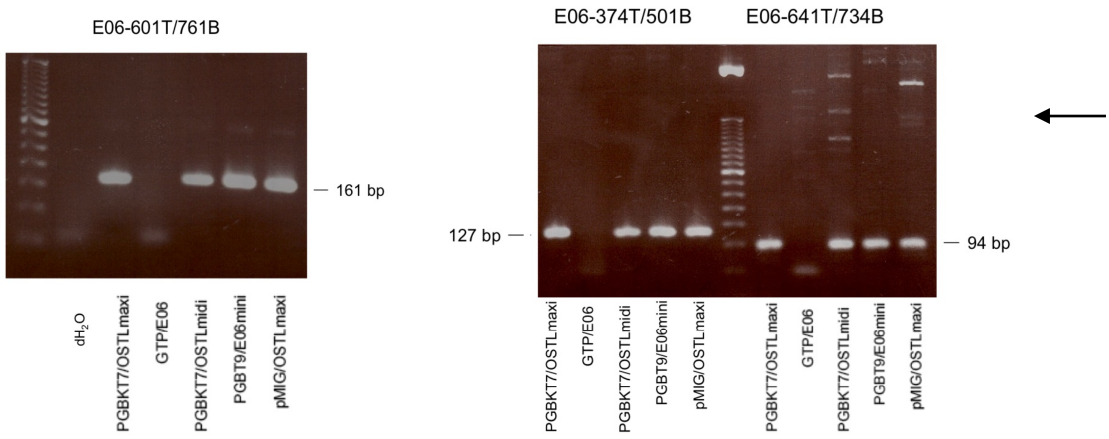

Figure 3.3: This PCR experiment was performed to investigate the primers' quality. We chose the annealing temperatures according to the base composition of the primers and set as displayed as follows: E06-374T/501B and E06-641T/734B: T_a= 54°C, E06-601T/761B: T_a= 57°C. The PCR product was visualized using a 1.5 % agarose gel. The expected size of the PCR product is marked on the side in base pares (bp). All PCR products appeared at the expected size. Only with E06-641T/734B extra bands appeared for most plasmids.

In the real-time PCR experiment, the reaction needs to work with much smaller concentrations of the target. Because of that, we diluted the plasmid pMIG/OSTL. We prepared the dilutions in 10-fold steps, so that we obtained final concentrations of 100 pg/µl, 10 pg/µl, 1 pg/µl, 0.1 pg/µl and 0.01 pg/µl.

Then we performed PCR. We always used 1 µl of each plasmid dilution per 20 µl PCR reaction mix. The annealing temperatures were set as above. We found that the fewer templates we added, the more unspecific products appeared at the size of 50 bp. A possible explanation would be primer dimers. As an example, the primer E06-641T/734B is shown in Figure 3.3.

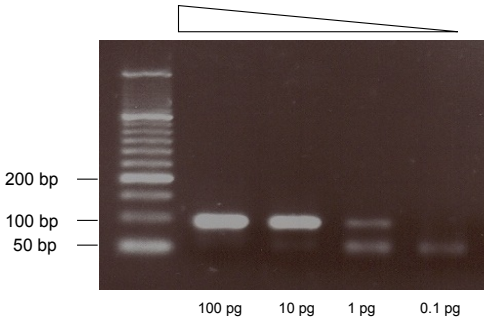

Figure 3.4: The PCR products of the PCR reaction with the primer E06-641T/734B are shown on a 1.5 % agarose gel. The annealing temperature for the reaction was 57°C. On the x-axis the amount of template DNA per reaction is stated. The template amount decreases in 10-fold steps from the left side to the right. PCR product appeared at the expected size of about 100 bp. In the reactions with 1 pg template and lower, an additional band is visible with a size of 50 bp, which could be primer dimers.

The appearance of potential primer dimers could have different reasons. One cause would be an inappropriate annealing temperature. This led us to our next step, where we tested diverse annealing temperatures. The result, however, was not convincing. Even more primer dimers were detectable as shown in Figure 3.5 for example.

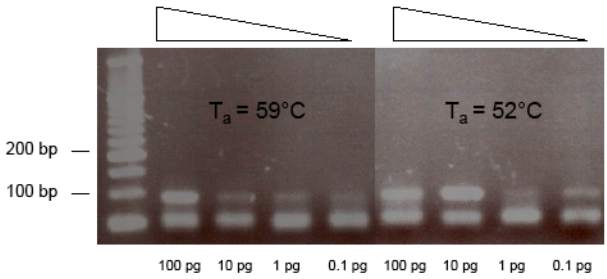

Figure 3.5: This figure depicts the PCR product of two dilution series. In both settings, the primer E06-641T/734B was used. Only the annealing temperature was adjusted to 59°C on the left side and to 52°C on the right side of the figure. Very strong primer dimers became visible in both settings.

The next attempt at eliminating the potential primer dimers was by adding Q-Solution to the reaction mix. Q-Solution is a PCR reaction additive, which

enhances amplification of templates that are GC-rich or that have extensive secondary structure. This solution modifies the melting behavior of nucleic acids. This also led to no improvement as is shown in the example Figure 3.6.

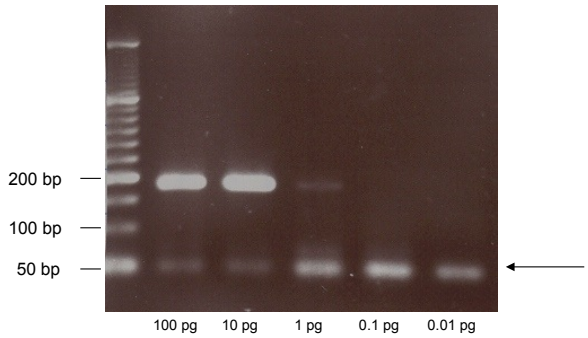

Figure 3.6: The figure depicts a 1.5 % agarose gel. The PCR product shown is received from the primer pair E06-196T/381B. The bands are expected at 180 bp. The annealing temperature used was 57°C. On the x-axis the amount of template DNA per reaction is indicated. Q-Solution was added to the reaction mix in order to enhance the amplification of the target sequence and to avoid unwanted amplification. But nevertheless additional products are visible at the size of about 50 bp especially in reactions with low template amounts (arrow).

Another reason for primer dimers could be an abundance of primers. In this way, unnecessary needless primers can form primer dimers. We prepared dilutions of the primers, although we used a primer concentration within the recommended range, namely 0.25 μM. We compared the concentration we normally used, 250 pM, with the final primer concentrations of the reaction mix of 125 pM, 50 pM and 25 pM. The PCR was performed in the usual program (T_a = 57°C) and 10 μg and 1 μg plasmid as template. As shown in Figure 3.7, the primer dimers disappeared in the higher dilution of primers.

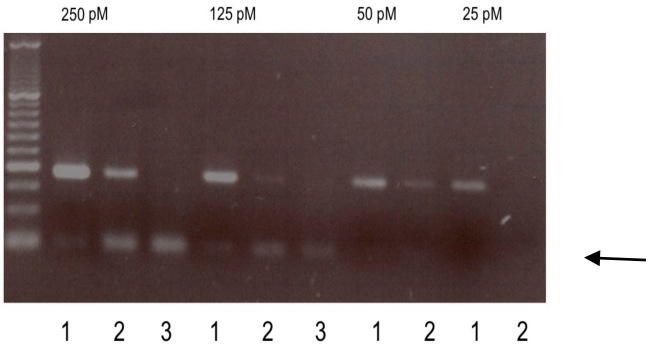

1 = pMIG/OSTL 10 pg, 2 = pMIG/OSTL 1 pg, 3 = dH_2O neg. control

Figure 3.7: Depicted in this figure is a 1.5 % agarose gel. The PCR products are visualized at the expected size between 150 bp and 200 bp. The PCR was performed with the primer pair E06-196T/381B in different dilutions and an annealing temperature of 57°C. The templates were plasmid pMIG/OSTL, 10 pg and 1 pg per reaction. In higher primer concentrations, again non-specific products appear at about 50 bp. But it is shown that the non-specific products disappear with lowering primer concentrations. At the concentration of 50 pM no products are detectable at 50 bp.

These difficulties in the establishment of the SYBR Green method bear too much insecurity to be a reliable experiment and this caused us to reject this method. We decided to use the TaqMan System.

3.2.1.2 TaqMan system

The TaqMan system is also often used for performing quantitative real-time PCR. It utilizes specific fluorogenic probes. Therefore it was necessary to design primers and corresponding fluorescent probes for the TaqMan System. For this we used Primer Express Software. The primer design for this technique follows the same rules as displayed for the SYBR Green System. In Primer Express Software, these and additional parameters for probe design are represented in a penalty score. Lower numbers indicate a primer/probe set that satisfies a greater percentage of the parameters contained in a list of requirements for the best possible result. This list includes the usual parameters required for primer design, such as GC content, melting temperature difference and primer and amplicon length. Probe specific conditions are also included, such as primer-probe distance. We only chose primer/probe sets with the lowest penalty score for each amplicon size. That means the primer constructed for an amplicon size of 101 bp had a penalty of

8 or 9. This applies to primer/probe sets OSTL-436/536, OSTL-783/883 and OSTL-861/961. The sets for the amplicon size of 51 bp, OSTL-574/647 had a penalty of 121, which is due to the very short amplicon length.

For the probe as well there are requirements that need to be considered in the design of the probe. It should also not exceed the GC percentage between 40 and 60 %. It should avoid runs of an identical nucleotide, especially of guanine. The probe should be located on the DNA strand, which lets the probe have more cytosine than guanine. The primer should be located as close to the probe as possible without overlapping. The probes are labeled with FAM reporter dye placed on the 5'-end. The non-fluorescent quencher BHQ-1 is placed on the 3'-end.

In Figure 3.8 the position of the expected amplicons and the corresponding primers is displayed in relation the exons of *OSTL*.

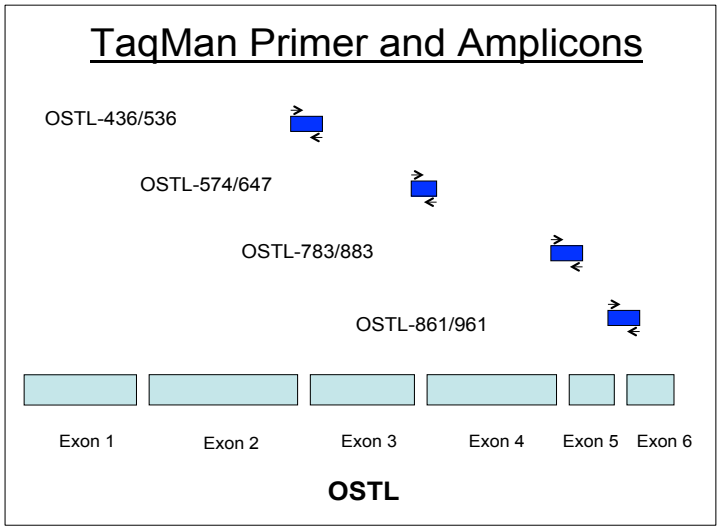

Figure 3.8: This figure depicts the primers' amplicons in relation to the exons of *OSTL*. The exons of *OSTL* are depicted in light blue. The amplicons are colored dark blue and the primers' names are written on the left side of the corresponding amplicon. Black arrows depict the primer.

The primers' performance was first analyzed in traditional PCR. Although appearing non-specific, structures such as primer dimer should not be a matter of concern using the TaqMan technique. We did not analyze OSTL-574/647,

because the expected amplicon would have a size of 51 bp. This would be very difficult to differentiate between the actual product and primer dimers, which both would appear at about 50 bp. We performed a PCR with the primer pairs OSTL-861/961, OSTL-783/883 and OSTL-436/536 using 100 pg pMIG/OSTL and pGBKT7 plasmids as templates (see Figure 3.9). The settings were standard and the annealing temperature was adjusted to 55°C. The results were satisfying, apart from OSTL-861/961in the reaction with plasmid pGBKT7. In this reaction, the band appeared at about 200 bp instead of the expected 100 bp. This primer pair spans the junction between exon 5 and 6. Concluding from that, the finding might be explained by a splice variant existing in this area (L Fontanari Krause, 2006). In this case, pMIG contains one variant and pGBKT7 another one.

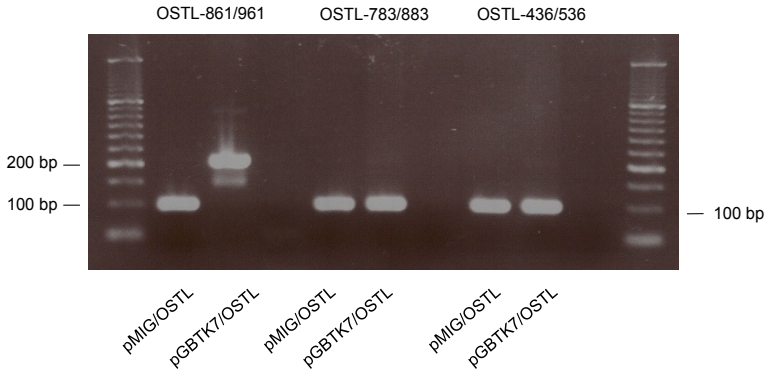

Figure 3.9: This figure depicts a 1.5 % agarose gel. Displayed are the PCR products using the primer pairs for TaqMan PCR: OSTL-861/961, OSTL-783/883 and OSTL-436/536. As template we used order pMIG/OSTL, then pGBKT7 plasmids (both times 100 pg per reaction) and bidest. water as negative control. All primers were designed to produce an amplicon at the size of 101 bp. As visible in the figure all PCR products have the expected size. Only the primer pair OSTL-861/961 shows a band at a size of around 200 bp in the reaction with pGBKT7 as template.

Figure 3.10 displays the performance of the primers under lower template concentrations. For this, we prepared different dilutions of plasmid pMIG/OSTL in 10-fold steps starting with 10 pg/μl down to 0.01 pg/μl. With all primer pairs, amplification of the amplicons is detectable in all concentrations. Only with OSTL-861/961 there was no amplification measurable in the reaction using 0.01 pg of

template. Non-specific products are only detectable in the reaction with the lowest concentration of template or in the negative control.

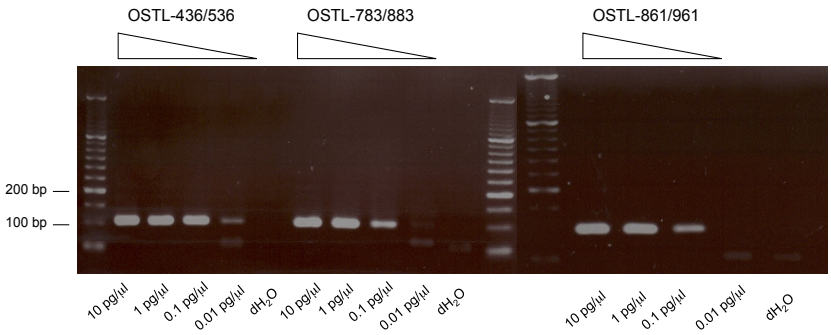

Figure 3.10: In this figure, the products of PCR reactions with the TaqMan primer pairs are displayed on a 1.5% agarose gel. Different amounts of template were added, from 10 pg plasmid in the left lane over 1 pg and 0.1 pg to 0.01 pg plasmid DNA per PCR reaction. For each primer pair, in the fifth lane no template is added as negative control.

In the last experiment before we proceeded to the actual real-time PCR experiments, we performed a PCR experiment with cDNA of different cell lines as template. We compared the performance of the primer pairs in cDNA, which will be the actual template in the real-time PCR experiments, and in plasmids. The cDNA was transcribed from RNA, which was extracted from the SEM, LCL B and DG75 cell lines. SEM is a Precursor B cell of type B-I. LCL B derives from lymphoblastoid cells. DG75 is a cell line of human Burkitt's Lymphoma cells.

The PCR was performed with the primer pairs OSTL-783/883, OSTL-861/961. In the DG75 cell line we also used *GAPDH* primer as positive control (see Figure 3.12). In SEM the signal visualized in the agarose gel almost equals the signal detected from the plasmids' products. With the primer pair OSTL-861/961 two bands appeared on the agarose gel, one stronger band at the expected size of about 100 bp and a weaker band at about 200 bp. The 200 bp band is detectable at the same size as with the plasmid pGBKT7, whereas the 100 bp band is in the range of pMIG/OSTL (see Figure 3.11). This is again most likely due to the known splice variant of *OSTL* in the location of the amplicon.

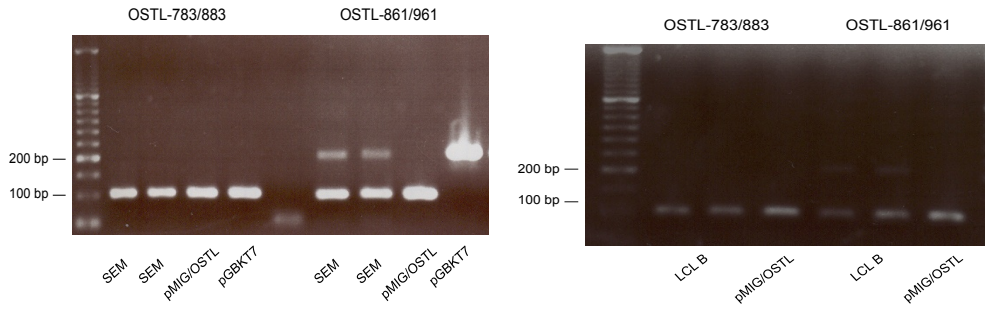

Figure 3.11: The figures depict the PCR products of the primer pairs OSTL-783/883 and OSTL-861/961. Annealing temperature was set to 55°C and 35 cycles were performed. cDNA from the SEM and LCL B cell lines, as well as plasmid pMIG/OSTL and pGBKT7 were used as template. All products appear at the presumed size marked by a 50 bp ladder, except OSTL-861/961 in plasmid, pGBKT7, that was visualized at about 200 bp. In both cell lines with OSTL-861/961 an additional weaker band is detectable at 200 bp to the expected 100 bp product.

In the experiment with the DG75 cell line, no products of *OSTL* were amplified.

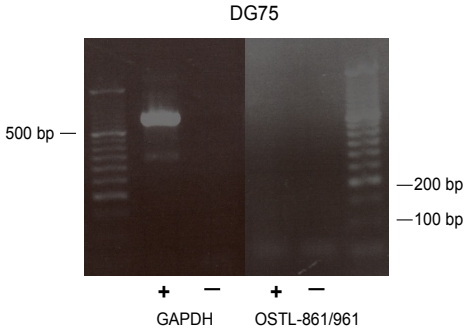

Figure 3.12: This figure displays the PCR results of OSTL-861/961and *GAPDH* primers. As template we used cDNA from the DG75 cell line. For the reaction with *GAPDH* primers, we used an annealing temperature of 60°C and 30 cycles. For OSTL-861/961 Ta was set to 55°C and 35 cycles were performed. Despite the higher cycle number, we were not able to amplify any product with OSTL-861/961 primers from the cDNA of DG75.

3.2.2 Real-time PCR experiments (TaqMan system)

3.2.2.1 TaqMan primer efficiency

After pre-examining the primer pairs in detail, we analyzed the primers' and the probes' efficiency in the TaqMan system. In order to do so, we performed standard curve analysis with all primer/probe sets. For this, the threshold cycles (C_t-values)

were determined for a set of dilutions. The threshold cycles were then plotted against the logarithm of the template concentrations. If the dilution series are prepared in 10-fold steps, the slope should ideally be -3.32.

The efficiency itself can be calculated from the slope with the Equation 3.1.

$$E_X = 10^{(-1/slope)} - 1$$

Equation 3.1: This equation was used for calculating the efficiency of the primer/probe sets. E_x represents efficiency. The slope is achieved by standard curve experiments.

We prepared dilution series in 10-fold steps of the plasmid pMIG/OSTL and of cDNA. The cDNA was transcribed from RNA of the SEM cell line.

The results we generated varied a lot over the different primer/probe sets. In the following paragraphs, the performance of each primer pair is described.

OSTL-436/536:

We performed real-time PCR and used dilutions from 100 ng/µl, 10 ng/µl, 1 ng/µl to 0.1 ng/µl. This means in the reaction where we added 100 ng, we had about 1x 10^{11} molecules in the reaction that hold the target sequence. But even with these high amounts, several adjustments and in several repeats, almost no amplification was detectable, neither in the plasmid nor in the cDNA cell line. With these poor results, we were not able to generate a reliable plot.

OSTL-574/647:

Here again we used 100 ng/µl, 10 ng/µl, 1 ng/µl and 0.1 ng/µl dilutions for the real-time PCR experiment. For this very high amount of molecules, low C_t-values could be expected. We used plasmids as template at first. However, using the primer/probe set OSTL-574/647 we only received C_t-values between 32 and 35 and found a high variance over the replicates of the same dilution. When we

plotted the C_t-values against the log quantity, we obtained a slope of -0.6216 (see Figure 3.13). From this slope we calculated the efficiency using the Equation 3.1. The estimated efficiency was 39.62%.

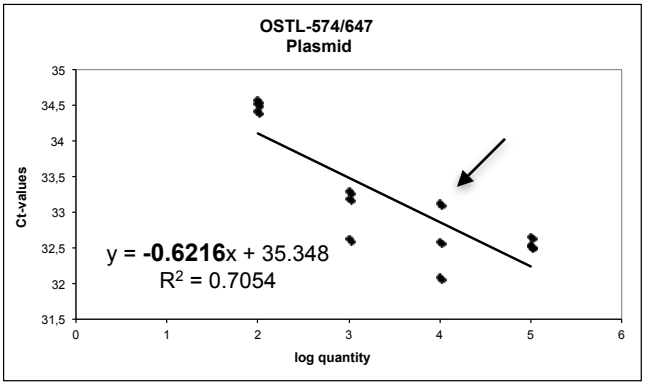

Figure 3.13: In this chart we plotted the threshold cycles generated with primer/probe set OSTL-574/647 against the logarithm of the template concentration. The template was plasmid pMIG/OSTL in the concentrations 100 ng/µl, 10 ng/µl, 1 ng/µl and 0.1 ng/µl. The slope generated from the plot was -0.6261 and marked in bold. The high variance within the triplicates is apparent. The most extreme example is marked with an arrow.

OSTL-783/883:

We performed standard curve analysis as well with the primer/probe set OSTL-783/883. For the first experiment with pMIG/OSTL, we used the following concentrations: 100 ng/µl, 10 ng/µl, 1 ng/µl and 0.1 ng/µl. Using these high amounts of molecules, we received C_t-values of 4 up to 15. To make the plasmid experiment more comparable with the one with the cDNA, we diluted the plasmid to 10 pg, 1 pg, 0.1 pg and 0.01 pg per reaction and the cell line cDNA 100 ng, 10 ng and 1 ng per reaction. Then we plotted the C_t-values against the logarithm of the concentrations. From these plots we generated the slope (see Figure 3.14). For the plasmid dilution we received a slope of -3.3536 and for the cDNA dilutions -3.922. With these slopes we calculated the efficiency using the Equation 3.1. We obtained an efficiency of 99% for the plasmid dilutions and 80% for the cell line dilution.

A

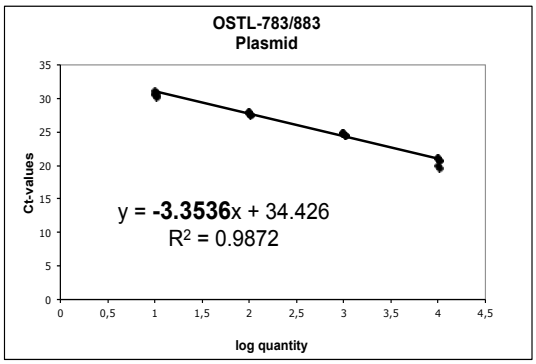

B

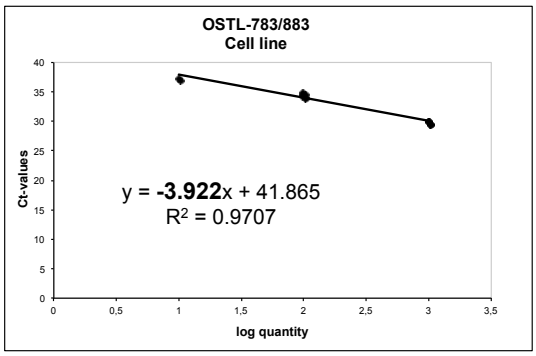

Figure 3.14: These figures display linear functions. They were achieved by plotting the C_t-values of a set of dilutions against the logarithm of the added quantity of target. The slope of the function is marked in bold. In Figure 3.14 A the template was pMIG/OSTL in the concentrations: 10 pg/µl, 1 pg/µl, 0.1 pg/µl and 0.01/µl. For Figure 3.14 B we utilized cDNA from SEM cell line in the following concentrations: 100 ng/µl, 10 ng/µl and 1 ng/µl. It is apparent that the triplicates of one dilution varied far less in their C_t-values than for example with primer/probe set OSTL-574/647.

OSTL-861/961:

With this primer/probe set, we proceeded in the same way as with OSTL-783/883. We first used high concentrations of the plasmid pMIG/OSTL (100 ng/µl, 10 ng/µl, 1 ng/µl and 0.1 ng/µl) and also received C_t-values between 5 and 18. For better comparability, we used lower dilutions of the plasmid and higher concentrations of the cDNA. But with 1 ng/µl, we could not detect any amplification. We found a slope of -3.4571 for the plasmid dilutions and a slope of -4.5731 for the cell line dilutions (see Figure 3.15). With this information, we calculated the efficiency using the Equation 3.1. The result for the plasmid dilutions was 95%, for the cell line 65%.

A

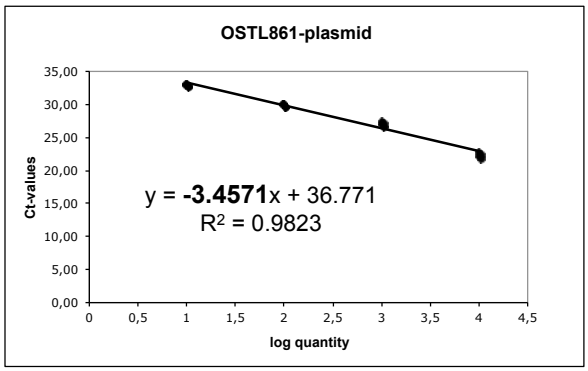

B

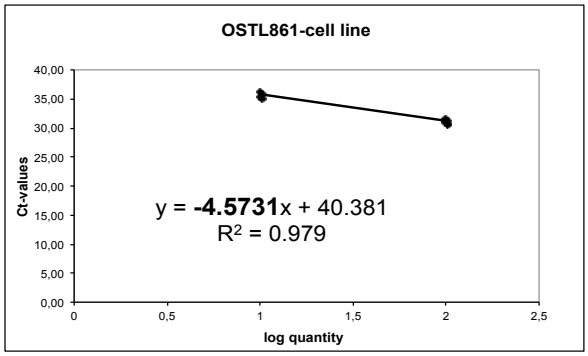

Figure 3.15: This plot is generated by plotting the C_t-values of a standard curve experiment against the logarithm of the quantity added. In Figure 3.15 A, plasmid pMIG/OSTL was used as template in the concentrations: 10 pg/µl, 1 pg/µl, 0.1 pg/µl and 0.01/µl and in Figure 3.15 B, the template was cDNA of the SEM cell line in the concentrations: 100 ng/µl, 10 ng/µl and 1 ng/µl. No amplification was detectable for the reactions with 1 ng template.

To decide which primer/probe set we should use for the relative quantification experiments, we took all the results from the traditional PCR experiments into consideration as well as the efficiency calculations. The sets OSTL-436/536 and OSTL-574/647 were excluded because of the poor performance in the standard curve analysis. We rejected OSTL-861/961 because of the splice variant in the area where the probe anneals. Also the efficiency was not as good as with OSTL-783/883. Thus we decided to use the primer/probe set OSTL-783/883 for the relative quantification experiments.

3.2.2.2 Normalization

To obtain objective and valid results, the generated data are normalized with control genes. These internal control genes function as an active reference and can normalize differences in the amount of cDNA.

We chose the control genes *β-Actin*, *GUSB* (Glucuronidase, beta) and *TBP* (TATA-binding protein). *TBP* showed a very low and unreliable expression pattern or was not expressed at all. Therefore it was excluded from the experiment.

Figure 3.16 depicts the C_t-values generated with the primer/probe sets for *OSTL*, *β-Actin* and *GUSB*. We compared the average threshold cycles of the control genes with the values of *OSTL* and decided to use *β-Actin* for normalization of the following experiments.

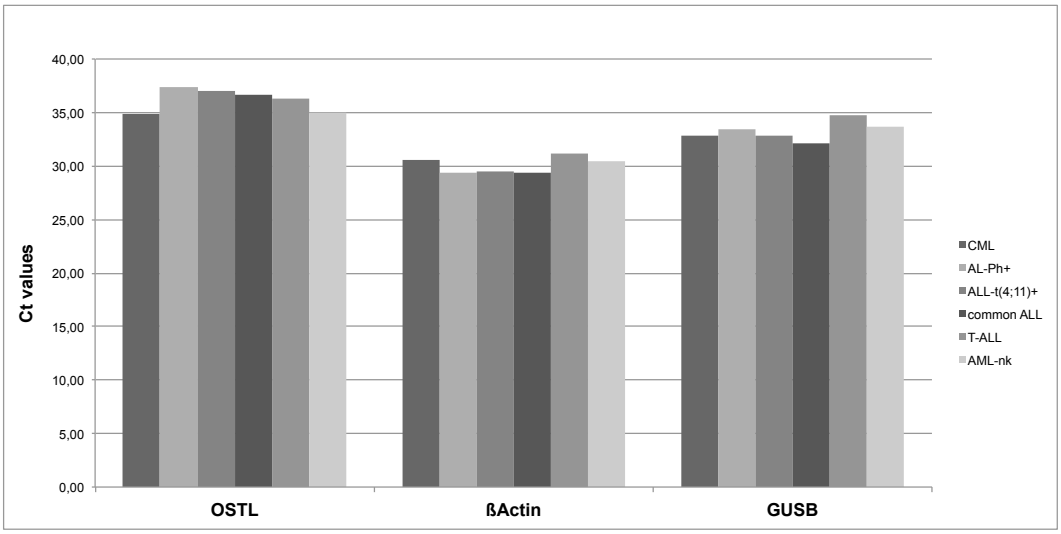

Figure 3.16: This figure depicts the raw C_t-values generated using the OSTL-783/883, *β-Actin* and *GUSB* primer/probe sets. Each column represents the average C_t-value of a group of patients with a certain leukemia. The groups comprise, from left to right, CML, AML (normal karyotype), T-ALL, common ALL, ALL-t (4;11) and ALL-Ph+.

3.2.2.3 Patients

The study includes 10 patients with CML, 10 AML patients with normal karyotype (AML-nk) and 20 ALL patients that can be divided into 4 subgroups (5 samples of ALL, Philadelphia Chromosome positive (ALL-Ph+); 5 patients with the

translocation t(4;11); 5 patients with common ALL and 5 patients with T-ALL). One of the ALL-Ph+ samples had to be excluded due to too-little an amount of cDNA. Therefore the ALL-Ph+ group only contains 4 samples.

The Table displaying the individual patients included in the relative quantification experiments can be found in the Appendix.

3.2.2.4 Relative quantification

ΔC_t-values

For relative quantification of the expression levels of the *OSTL* gene, we performed real-time PCR. We acquired the data of these experiments as outlined in the Methods section. The C_t-values of *OSTL* of every patient were normalized with the β-Actin C_t-values of the corresponding samples. This resulted in a ΔC_t-value. Smaller ΔC_t-values indicate higher expression and higher ΔC_t-values therefore lower expression.

Figure 3.17 shows the ΔC_t-values of *OSTL* of every individual patient sample. CML patients appear with the smallest ΔC_t-values, which means the highest expression. Whereas the ALL samples show overall lower expression indicated through generally higher ΔC_t-values. The ALL subgroups appear with heterogeneous expression levels.

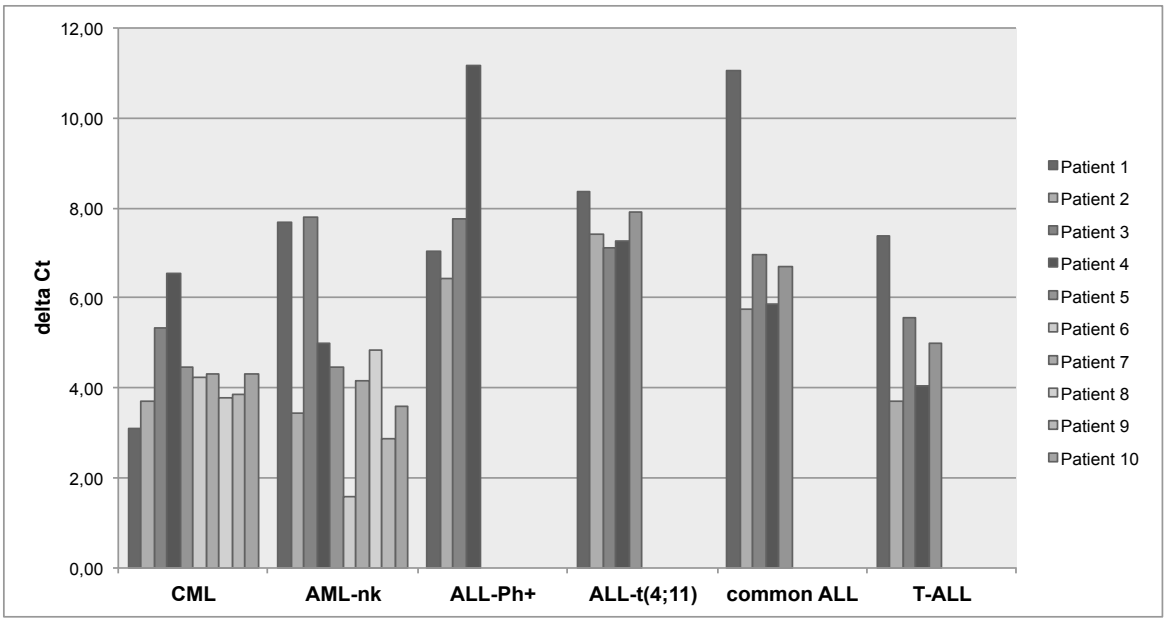

Figure 3.17: This figure displays the individual ΔC_t-values of *OSTL* in every patient sample. The ΔC_t-values are normalized with the control gene β-Actin. The patient samples are grouped in the underlying diseases. Depicted are the expression levels of 10 CML patients, 10 AML patients and 19 ALL patients. The ALL patients are divided into subgroups as follows: 4 patients with ALL, Philadelphia Chromosome positive; 5 patients with the translocation t(4;11); 5 patients with common ALL and 5 patients with T-cell ALL.

Figure 3.18 demonstrates the average ΔC_t-values of every leukemia subgroup and the corresponding standard deviation. The myeloid leukemia, CML and AML appear with the lowest ΔC_t-values (CML 4.36; AML 4.55) meaning the higher expression. Only in AML the standard deviation is wider, indicating the highest variance over the individual samples. The highest ΔC_t-values appear in ALL subgroups (in descending order: ALL-Ph+: 8.09; ALL-t(4;11): 7.62; common ALL: 7.27). An exception in the ALL subgroups is the T-ALL subgroup. The expression of *OSTL* in the T-ALL patients is, with 5.14, more similar to CML and AML than to the other ALL samples.

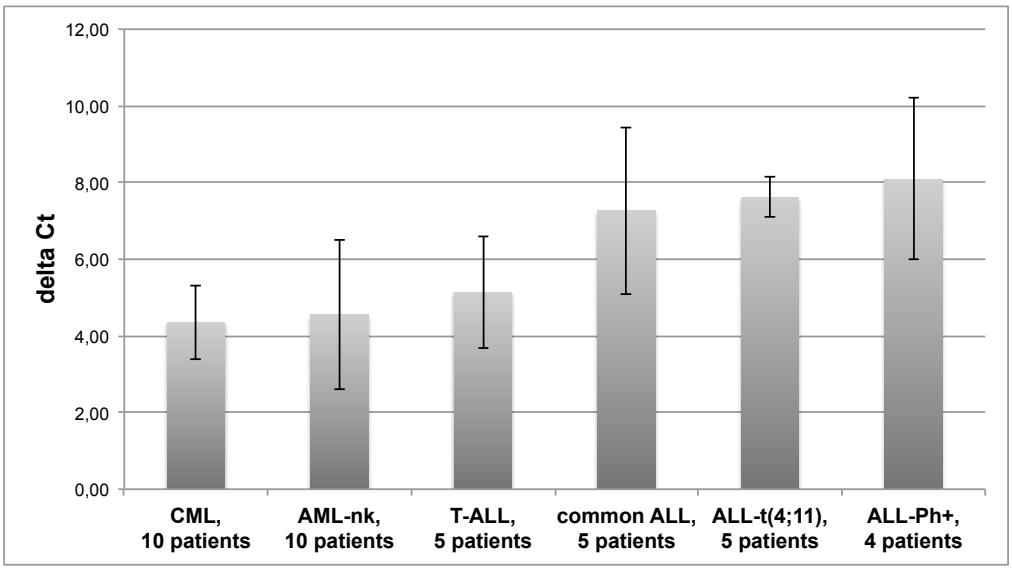

Figure 3.18: This figure depicts the average ΔC_t-values of *OSTL* in CML, AML and all ALL (T-ALL, common ALL, ALL-t(4;11), ALL-Ph+). Grey columns represent the ΔC_t-values. The ΔC_t-value is an indicator for the expression. Black bars indicate the standard deviation. All values were normalized with the control gene *β-Actin*.

In Figure 3.19 all ALL subgroups are summarized in one group. Still the expression of *OSTL* in the average of all ALL subgroups is lower than AML and CML implicated by the higher ΔC_t-value (7.03). CML and AML express *OSTL* almost equally. Only the standard deviation is higher for the AML (1.96) samples compared to CML (0.97). The standard deviation of AML almost equals the standard deviation of the ALL group (1.92).

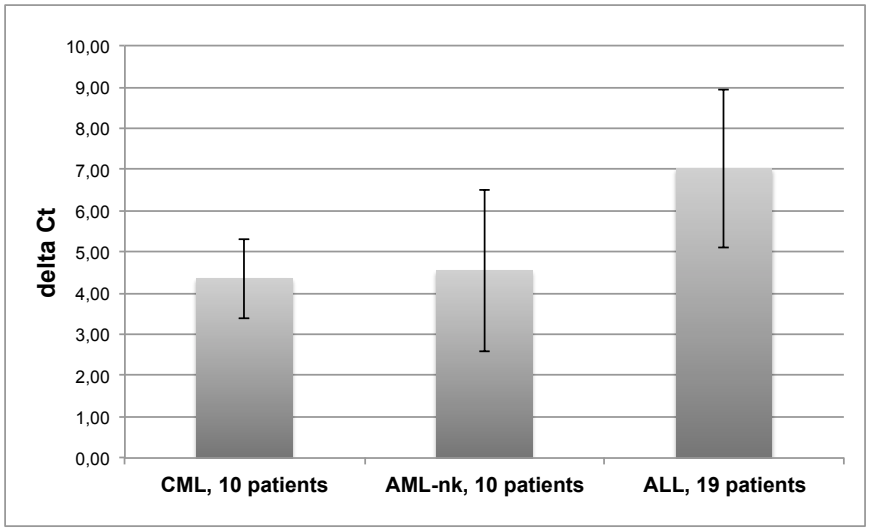

Figure 3.19: This figure depicts the average ΔC_t-values of *OSTL* in CML, AML and all ALL subgroups summarized in one group. The grey columns represent the ΔC_t-values. The ΔC_t-value is an indicator for the expression. Black bars indicate the standard deviation. All values were normalized with the control gene *β-Actin*.

$\Delta\Delta C_t$-values

The following part displays the comparison of *OSTL* expression in the different types of leukemia. Basically, this method contrasts the expression levels (described in ΔC_t-values) with a reference (also described in ΔC_t-values). This results in the difference between ΔC_t-values, which are represented as $\Delta\Delta C_t$-value. Positive $\Delta\Delta C_t$-values represent lower expression than the reference. In this way, negative $\Delta\Delta C_t$-values indicate higher expression than the reference. Higher $\Delta\Delta C_t$-values represent a greater difference between the sample and the reference.

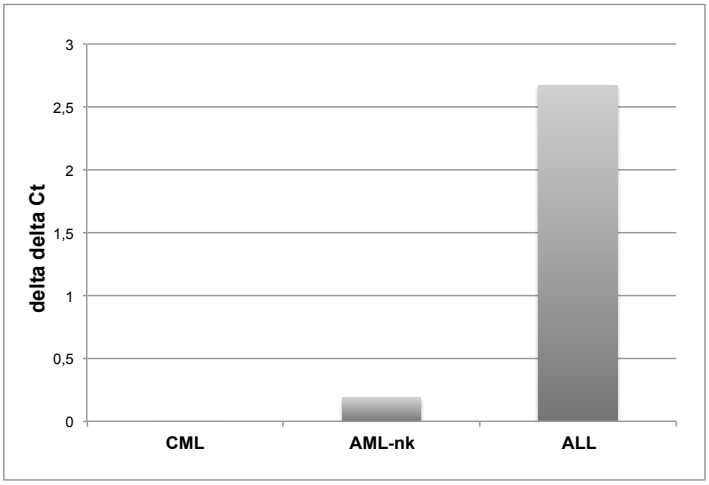

Figure 3.20: This figure depicts the relative quantification of AML (normal karyotype) and ALL. The reference is CML. The columns indicate $\Delta\Delta C_t$-values. They are the difference between the sample and the reference.

Figure 3.20 represents a relative quantification. CML is set as reference and compared to AML and ALL. The *OSTL* expression in AML almost equals its expression in CML, which is shown by the very low $\Delta\Delta C_t$-value (0.19). The $\Delta\Delta C_t$-value of ALL in this figure is higher, with 2.67, indicating a lower expression.

$$\textbf{Fold change} = 2^{\Delta\Delta Ct}$$

Equation 3.2: With this equation the fold change between two expression levels can be calculated. $\Delta\Delta C_t$ describes the difference between the two ΔC_t-values of the two compared values. The equation is based on the theory that every PCR amplicon doubles in every PCR cycle.

Equation 3.2 is used to calculate fold differences between sample and reference. It assumes an efficiency of 100%. However, in the standard curve experiment for the primer/probe set OSTL-783/883, the efficiency was only 80%. Taking this into consideration, the Equation 3.2 has to be adjusted as shown below:

$$\textbf{Fold change} = 1.8^{\Delta\Delta Ct}$$

Equation 3.3: The equation is based on Equation 3.2. It takes the actual efficiency of 80% for primer/probe set OSTL783/883 into consideration.

Taking this into consideration, *OSTL* is expressed 4.8-fold higher in CML than in ALL.

Because the ALL subgroups varied in the expression as shown in Figure 3.21, all ALL subgroups are depicted separately. The $\Delta\Delta C_t$-values compared to CML differ between the ALL subgroups from 0.78 in T-ALL to 3.73 in ALL-Ph+. This means that there is only a 1.58-fold difference between T-ALL and CML but almost a 9-fold difference between ALL-Ph+ and CML.

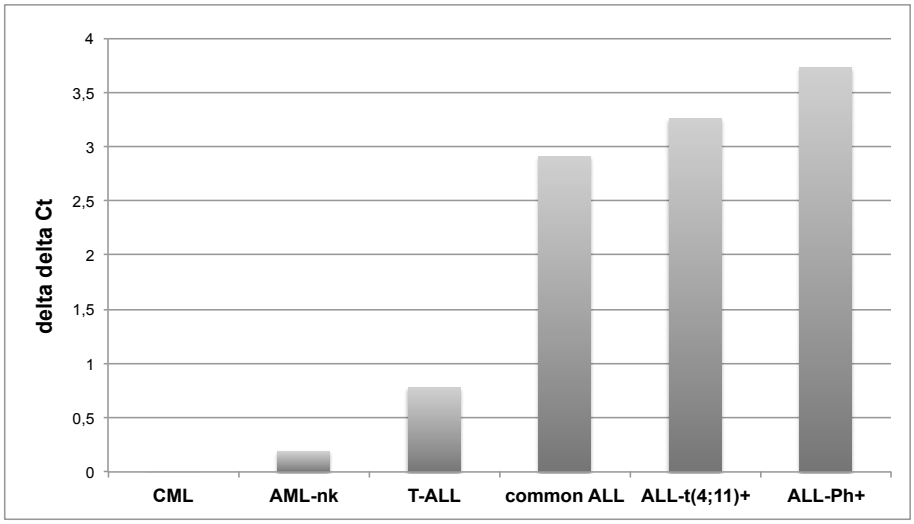

Figure 3.21: This figure depicts the relative quantification of *OSTL* expression in AML-nk, T-ALL, common ALL, ALL-t(4;11) and ALL-Ph+. The reference is CML. The columns indicate average $\Delta\Delta C_t$-values of all groups. They represent the difference between the sample and the reference.

Figure 3.22 represents the relative quantification of CML, AML, common ALL, ALL t(4;11) and ALL-Ph+ with the reference T-ALL. AML and CML express *OSTL* at a higher level than T-ALL shown by the negative $\Delta\Delta C_t$-values. But the expression level is only 1.41-fold higher in AML and 1.58-fold in CML. In all other ALL subgroups, *OSTL* is expressed as lower than T-ALL. The expression level is 3.5- fold higher in common ALL, 4.3-fold in the ALL with the translocation t(4;11) and 5.66-fold in ALL.

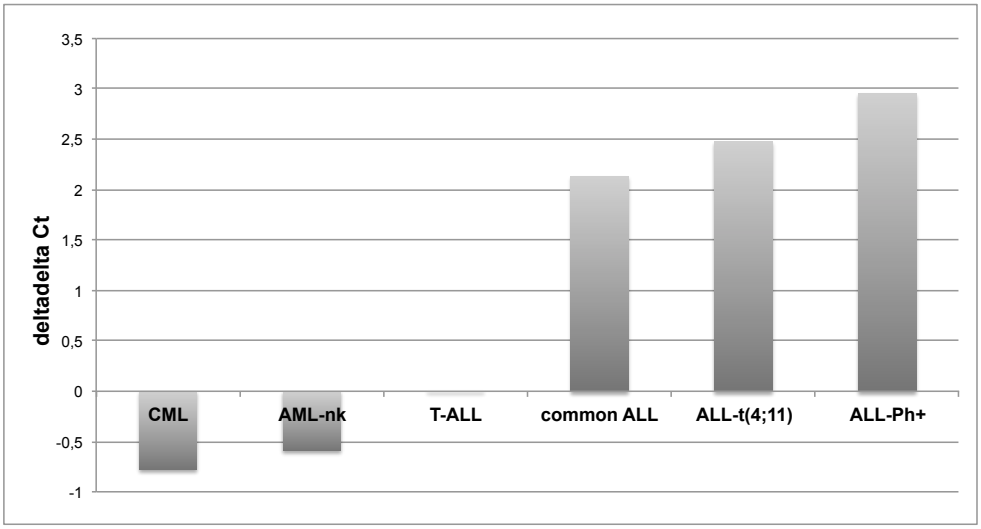

Figure 3.22: This figure depicts the relative quantification of the *OSTL* expression in CML, AML-nk, common ALL, ALL-t(4;11) and ALL-Ph+. The reference is T-ALL. The columns represent $\Delta\Delta C_t$-values. They represent the difference between the sample and the reference. Negative $\Delta\Delta C_t$-values indicate higher expression than the reference. Positive bars represent lower expression than the reference.

4 Discussion

OSTL was discovered adjacent to the 6q23 breakpoint of the translocation t(6;12)(q23;p13), which leads to the *ETV6/STL* fusion gene. This translocation involves *ETV6,* which is known to be associated with leukemia development. Usually *ETV6* fusion genes lead to the generation of a fusion protein with altered function. However, this is not the case with the *ETV6/STL* fusion. The *ETV6/STL* fusion as well as the reciprocal fusion *STL/ETV6* only code for small proteins with unknown function (Y Suto, 1997). This led the focus of interest to the *OSTL* gene that is next to *STL* on the long arm of chromosome 6. *OSTL* shares the first exon with *STL*. But *OSTL* is transcribed in the opposite direction to *STL*.

Figure 4.1 demonstrates the relationship of the genes *ETV6, STL* and *OSTL* on Chromosomes 6 and 12 under normal conditions and with the translocation t(6;12)(q23;p13).

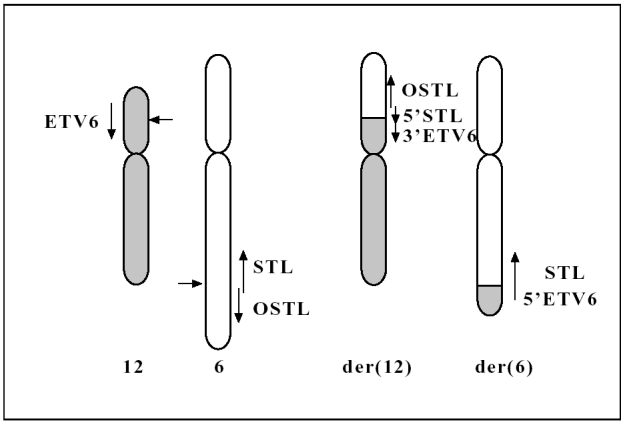

Figure 4.1: This figure depicts Chromosomes 6 and 12. *ETV6* is located on the short arm of Chromosome 12, whereas *STL* and *OSTL* are localized on the long arm of Chromosome 6. *STL* and *OSTL* are transcribed in opposite directions but share the first exon. On the right, the translocation t(6;12)(q23;p13) is shown. It results in an *ETV6/STL* and an *STL/ETV6* fusion. *OSTL* is not directly affected by the translocation. Adapted from L Fontanari Krause, 2006.

Fontanari Krause et al. have examined the *OSTL* gene in detail. They discovered interesting characteristics of *OSTL*, which allow the hypothesis that *OSTL* plays a role in leukemogenesis. *OSTL* contains a RING-IBR-RING/TRIAD motive that

functions as E3 ubiquitin ligase in other proteins (AD Capili, 2004). But Fontanari Krause et al. could not show an ubiquitin ligase function of OSTL. The human and the mouse OSTL are highly conserved which suggests that OSTL has an evolutionary important function in the cell. The OSTL protein is localized mainly in the cytoplasm and it is not restricted to a single tissue. *STL* shows the same expression pattern as *OSTL*, which suggests co-expression. *OSTL* is also detectable during all stages of B-cell development. This could be an indicator that *OSTL* also plays a role here. It could also be detected during certain periods of mouse embryogenesis, which suggests that *OSTL* is also involved in embryogenesis.

Fontanari Krause et al. identified the proteins HAX-1 and SIVA as interaction partners of OSTL. Both proteins are involved in apoptosis, suggesting that OSTL also has a role in apoptosis.

We studied the expression levels of *OSTL* in different types of leukemia to identify a correlation of *OSTL* with a leukemia subtype. We anticipated an increased expression of *OSTL* in ALL patients. This assumption is based on the fact that the translocation was detected first in a young patient with pre-B-cell ALL (Y Suto, 1997). In addition *OSTL* was mainly expressed in cells of the lymphatic system (L Fontanari Krause, 2006).

4.1 Assessment of the results

We first used microarray data from 129 patients with different types of leukemia (CML and 12 different Acute Leukemia) and normal bone marrow to obtain an overview of *OSTL* expression levels. These analyses showed that *OSTL* was expressed twice as high in CML patients compared to samples from normal bone marrow, AML or ALL samples.

To validate these results we conducted real-time PCR experiments on 39 leukemia patient cDNA samples, CML showed the highest expression of *OSTL*, which supports the findings of the microarray analysis. However, the expression level of *OSTL* in the CML group was almost identical to the AML group (see Figure 3.20). Both groups include 10 patients. This offers a good comparability. Though

these groups are relatively small, the AML group is genetically more heterogeneous than the CML group.

It is of interest that, in earlier experiments, *OSTL* seemed to play a bigger role in the lymphatic lineage than in the myeloid (L Fontanari Krause, 2006). This makes it even more surprising that we found the highest expression of *OSTL* in myeloid leukemia. Our real-time PCR experiments confirmed the results of the microarray analysis that *OSTL* is expressed at lower levels in ALL than in myeloid leukemia, especially CML.

To be precise, *OSTL* is expressed 4.8-fold lower in ALL patients than in CML patients. The ALL group contains 19 patients and is divided into 4 subgroups: common ALL, ALL with a t(4;11), T-ALL and ALL-Ph+. The ALL group also shows very heterogeneous *OSTL* expression levels. We expected the highest *OSTL* expression in the ALL-Ph+ since ALL-Ph+ patients, like CML patients, have a t(9;22)(q34;q11) translocation leading to the *BCR/ABL* fusion gene (A deKlein, 1982; JD Rowley, 1973).

Very much to our surprise, ALL-Ph+ patients express *OSTL* at a 9-fold lower level than CML patients. In contrast to this, T-ALL patients show very high *OSTL* expression levels, which are almost equal to the expression levels observed in myeloid leukemia. The fold change between T-ALL and myeloid leukemia is only 1.5. Common ALL and ALL-t(4;11) patients have intermediate expression levels. They express *OSTL* 5.5-fold and 6.7-fold lower than CML patients, respectively (see Figure 3.21).

However, both the microarray analyses and the real-time PCR measurements detected the highest expression of *OSTL* in CML patients. Only the fold differences varied between the two methods.

4.2 Discussion of the results

Genetic alterations are the basis of leukemogenesis (T Burmeister, 2000; U Krug, 2005; H Lodish, 2007; F Mitelman, 2007; JD Rowley, 1999). Translocations play an important role, resulting in either the formation of fusion genes (e.g. *BCR/ABL*)

or the deregulation of gene expression (e.g. overexpression of *MYC* as the consequence of the t(8;14) translocation). Fusion genes result in altered or enhanced function of the genes involved. They frequently affect tyrosine kinases or transcription factors (SK Bohlander, 2000; T Burmeister, 2000; U Krug, 2005; H Lodish, 2007; F Mitelman, 2007).

However, the distinction between translocations resulting in fusion genes or in deregulated gene expression is sometimes not easy, since there are apparently genes that can be involved both in translocations leading to the formation of fusion genes and in translocation leading to the overexpression of breakpoint adjacent genes. One such gene is *ETV6* (SK Bohlander, 2005).

An example of overexpression of a gene as the driving force in tumorigenesis is, among others, *CDX2* that is involved in the rare t(13;12) translocation. Even though an *ETV6/CDX2* fusion transcript is produced, the main leukemogenic force is the overexpression of *CDX2*, which is also a result of this translocation (VPS Rawat et al., 2004). Subsequently it was shown that *CDX2* is also overexpressed in AML and ALL cases without the t(12;13) (VPS Rawat et al., 2008; S Thoene, 2008). In cell line experiments as well as in mouse models, Scholl et al. corroborated the theory of *CDX2* as a driving force in leukemogenesis (C Scholl, 2007).

Ectopic Expression of neighboring genes as a reason for leukemogenesis is also suspected in other translocations involving *ETV6*. For example, this is the case with the translocation t(1;12)(p36.1;p13), which was discovered in a patient with Myelodysplastic Syndrome (MDS). Here they hypothesized that altered expression of surrounding genes might be the MDS-inducing factor. Real-time PCR experiments showed that *RPL11*, a gene in close vicinity to *MDS2*, was expressed at higher levels in samples from patients with the t(1;12) than in normal bone marrow samples (MD Odero, 2002).

Panagopoulos et al. investigated a rearrangement of the 12p13 region in a case of pediatric pre-B ALL. The rearrangement involved *ETV6* and *BAZ2A*. The chimeric protein is also very short in length and very similar to the *ETV6/STL* and *ETV6/MDS2* fusions. So the *ETV6/BAZ2A* fusion was not expected to have any function. They rather hypothesized that the pathogenic mechanism is the

deregulation of *BAZ2A*. They assume *BAZ2A* comes under the control of either a cryptic promoter or the promoter of *ETV6* (I Panagopoulos, 2006).

Cools et al. studied the translocations t(4;12)(q11-q12;p13) and t(5;12)(q31;p13). In both cases, no functional fusion gene of *ETV6* could be identified. However they showed that the homeobox gene *GSH2* (4q11-q12) and the growth factor gene *IL3* (5q31) were ectopically expressed in these two cases, suggesting that these events might be the drivers of leukemogenesis (J Cools, 1999 and 2002).

The translocation t(6;12)(q23;p13) causes the generation of fusion genes of *ETV6* and *STL*. As in the cases of *CDX2*, *MDS2*, *BAZ2A* and *GSH2* that are described above, the leukemic effects of the translocation are not fully understood. Neither the *STL/ETV6* fusion nor the reciprocal *ETV6/STL* fusion shows a long open reading frame (ORF) (see Figure 4.2). The resulting fusion protein is, like the other examples, very small and lacks any known functional domain. No homologies to other known proteins could be observed (Y Suto, 1997). Therefore, as with the other examples, they assumed dysregulation of another nearby gene as a leukemogenic effect.

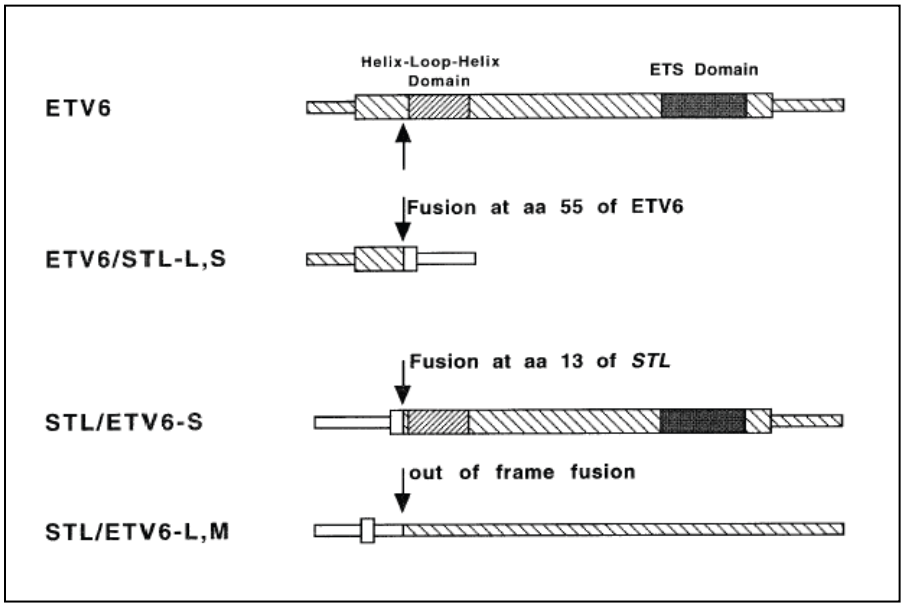

Figure 4.2: Here the *ETV6*, the *ETV6/STL* and the *STL/ETV6* protein structure are shown. Adapted from Y Suto et al., 1997.

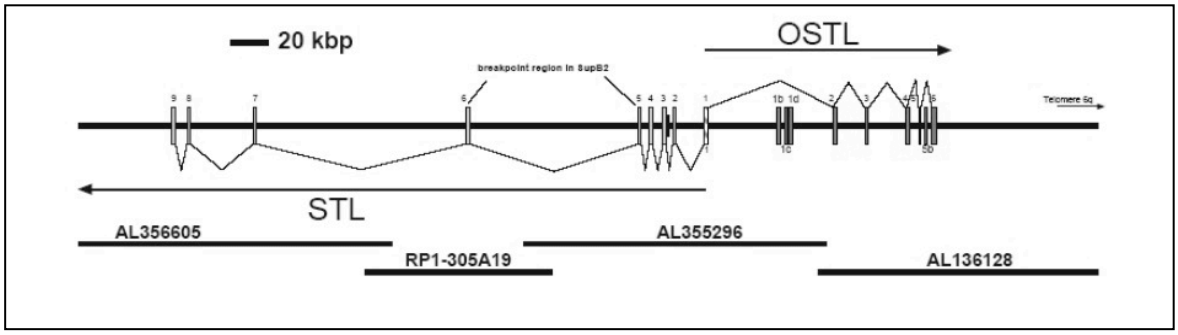

Figure 4.3: This figure depicts a map of the *STL/OST*L loci. It displays the close relation between *OSTL* and *STL*. *STL* exons are demonstrated by light grey bars; *OSTL* exons by dark grey bars. Black arrows indicate the direction of transcription. Black bars at the bottom of the figure represent the genomic sequence. Adapted from L Fontanari Krause, 2006.

In the case of t(6;12)(q23;p13), *OSTL* came into the focus of interest because it is located in the proximate vicinity of *STL*. *OSTL* even shares the first exon with *STL*. Figure 4.3 shows a map of the *STL/OSTL* loci to demonstrate the close relationship between the two genes.

Furthermore, it seems that *STL* and *OSTL* are co-expressed. Therefore, we performed an expression analysis of *OSTL* in various leukemia samples. Our studies showed a higher expression of *OSTL* in patients with AML and especially with CML. This was quite surprising, because up to that time *OSTL* had been thought to be more important in the lymphatic cell lineage. It is expressed during B-cell development and the t(6;12)(q23;p13) was first described in a pediatric case of B-cell precursor ALL (L Fontanari Krause, 2006; Y Suto, 1997; LQ Zhang, 1993). Therefore, our findings of the highest expression levels of *OSTL* in myeloid leukemia (especially CML) were interesting findings.

Due to these findings, we have to conclude that *OSTL* is also involved in the leukemogenesis or the progression of these diseases. However, the molecular mechanisms of how *OSTL* contributes to myeloid neoplasm are not known at present. The detailed studies of L Fontanari Krause give some insights into the function of *OSTL* and thus provide a basis for forming some hypotheses about the role of *OSTL* in tumorigenesis.

For example, Fontanari Krause et al. found that *OSTL* is also expressed during embryogenesis. This could mean that *OSTL* is involved in cell growth. In most

adult tissues the expression levels of *OSTL* are rather low. Therefore higher expression of *OSTL* in adult or leukemic cells might be an indicator that the normal cell physiology is disturbed. Alternatively, elevated expression of *OSTL* itself could be the reason for a disturbed cellular growth. This may also affect cell differentiation, proliferation or self-renewal, which are very sensitive processes in the cell regulation. Disturbance of these functions often results in malignant transformation (JK Warner, 2004; JA Kennedy, 2008). *OSTL* is thought to be involved in cell survival, which is also one of the processes that are frequently disturbed in malignant cells. For example, overexpression of *CDX2* is assumed to enhance the self-renewal capacity (C Scholl, 2007).

Also the interaction partners of OSTL bear the potential to mediate leukemogenic effects. These proteins have been shown to be HAX1 and SIVA (L Fontanari Krause, 2006).

HAX-1 (HS1 associated protein X-1) can be found in almost all tissues, suggesting a fundamental role in the cell. It is mainly localized in the mitochondria and has been associated with signal transduction as well as regulation of the actin cytoskeleton. It is believed that HAX-1 has anti-apoptotic properties and that it promotes cell survival (Y Suzuki, 1997; A Mirmohammadsadegh, 2003). Han et al. discovered that HAX-1 inhibits the processing of caspase 9 and thus prevents apoptosis in cardiomyocytes. This supports the hypothesis that HAX-1 has anti-apoptotic qualities (Y Han, 2006; J Shaw, 2009). Recently it was shown that HAX-1 is mutated in recessive severe congenital neutropenia (SCN; Kostmann disease). Klein et al. detected homozygous mutations in the *HAX-1* gene in several patients with SCN. It has been proposed that the lack of HAX-1 causes increased apoptosis in myeloid progenitor cells and that this could be a potential mechanism for neutropenia in patients with SCN (AA Schäffer, 2009; C Klein, 2006).

The second *OSTL* interactor that is of great interest is SIVA. Prasad et al. first described SIVA in 1997. SIVA (named after Shiva, the Hindu God of destruction) plays an important role in death vs. life decisions in the cell. SIVA interacts with various members of the tumor necrosis factor (TNF) receptor family (e.g. CD27, GITR, OX40 and 4-1BB) and shows pro-apoptotic properties (KV Prasad, 1997). Okuno et al. found that SIVA is upregulated in colorectal tumors (K Okuno, 2001).

Later it was shown that SIVA is an effector of p53 in apoptosis and that it is involved in the induction of apoptosis after the DNA is damaged (JL Barkinge, 2009). An isoform of SIVA, SIVA-1, also has negative regulatory potential on NF-κB and it is part of the T-cell receptor induced cell death (AICD, activation-induced cell death) (R Gudi, 2006).

The work of Fontanari Krause et al. shows that OSTL interacts both with HAX-1 and SIVA and might thus influence apoptosis and cell survival. Maybe the deregulation disturbs the pathways of HAX-1 and SIVA and in this way alters the normal regulation of apoptosis and cell survival. This hypothesis is depicted graphically in Figure 4.4. To understand the underlying mechanism, a more detailed characterization of the interaction between OSTL and HAX-1 and SIVA is required.

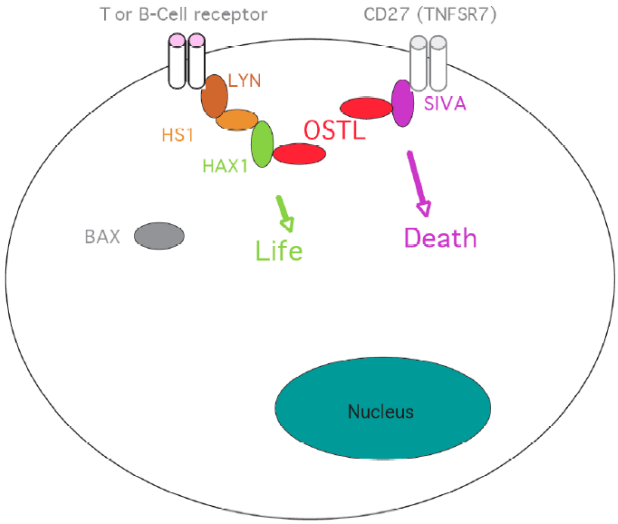

Figure 4.4: Fontanari Krause et al. worked out an interaction of OSTL with HAX-1 and SIVA. This figure demonstrates a potential mechanism of how the protein could relate in the cell. Adapted from L Fontanari Krause, 2006.

4.3 Discussion of the methods

4.3.1 Microarray analysis

Microarray analysis has been used since 1995 to analyze the expression levels of genes (M Schena, 1995). Using this method, a large number of genes or even all

genes can be assayed simultaneously. This allows an overview of the expression pattern of groups of genes or all genes in a given condition (R van Haaften, 2006). A disadvantage of this method is the high amounts of RNA that are needed per experiment. 20-200 μg RNA were necessary for one of the earlier microarray experiments and even now at least 100 ng of RNA are required per chip, whereas for real-time PCR, only a few nanograms of RNA are needed (V Nygaard, 2003). In addition, both sensitivity and specificity are higher for real-time PCR in comparison to microarray analysis (Y Chen, 2009).

Our initial microarray analysis included 129 patients with various types of leukemia and 10 samples with normal bone marrow. These data allowed us to determine a first rough trend of the expression levels of *OSTL* in leukemia. We used this analysis to get an overview of what we should expect in real-time PCR.

4.3.2 Real-time PCR (quantitative PCR)

The innovation of real-time PCR compared to traditional PCR is that the target sequence is not only amplified but also quantified during amplification. Real-time PCR is based on the principles of traditional PCR, but in real-time PCR the amplification of the DNA target can be observed in real-time. This has the advantage that the data are collected during the exponential phase of the amplification. This is the phase with the highest efficiency of the reaction and therefore offers the highest accuracy. And the exponential phase is not affected as much by confounding variables as the plateau phase. Thus the most reliable results can be obtained in the exponential phase (MT Dorak, 2006).

Even very small amounts of DNA can be detected and quantified reliably. The real-time PCR system requires 1000-fold less RNA than conventional methods and still less than microarray experiments. Thus very subtle changes in the expression levels of a given gene can be detected (MT Dorak, 2006).

4.3.2.1 SYBR Green versus TaqMan

There are basically two detection systems in real-time PCR. One is the SYBR Green system, which uses an intercalating dye that emits a different fluorescence,

when it intercalates in any double-stranded DNA (dsDNA). The other system is named TaqMan and utilizes specific probes.

In the SYBR Green system, the SYBR Green I fluorescent marker intercalates in all dsDNA. When intercalated, SYBR Green I emits fluorescence at a specific wavelength. The fluorescence intensity corresponds to the amount of dsDNA but is not specific for a target sequence. Because the SYBR Green I dye is not sequence-specific, assays with SYBR Green I require extensive optimization and post-processing (V van der Velden, 2003). The non-specific products could interfere with the results. The results would appear incorrectly high, as the non-specific products would also be detected as dsDNA in addition to the sequence of interest. Furthermore, a melting curve analysis is required as post-processing to verify the results. With melting curve analysis, it is possible to distinguish between specific and non-specific PCR products (KM Ririe, 1997).

The optimization of the PCR protocol for the SYBR Green system for the analysis of *OSTL* transcript levels turned out to be rather difficult. Primer dimers appeared despite all attempts to optimize the reaction. This system also had the risk of false results and we decided against this system and looked for a sequence-specific system.

Another system is the TaqMan system. This system uses hydrolysis probes. Hydrolysis probes are oligonucleotide sequences that bind DNA specifically at the area of interest between the primers. A quencher fluorochrome is conjugated to one end of the probe and a reporter fluorochrome to the other end. The quencher fluorochrome absorbs the fluorescence emitted by the reporter dye as long as both are bound in close proximity to each other. This is because of the FRET effect (Förster (or fluorescence) resonance energy transfer) (D Grinzinger, 2002). The Thermus aquaticus (Taq) polymerase hydrolyzes the probe with its 5’ → 3’ exonuclease activity during the elongation step of the PCR cycles. Thereby the quencher and the reporter are separated. This way the FRET effect is lost and the reporter emits fluorescence of a specific wavelength. The emitted fluorescence rises proportionally to the increasing amount of target DNA in the reaction. Interference by non-specific amplification products does not occur (V van der Velden, 2003). A schematic representation of both systems is depicted in Figure 4.5.

The TaqMan system is more specific in comparison to the SYBR Green system and it does not require as much optimization or any post-processing. These facts made us decide in favor of the TaqMan system.

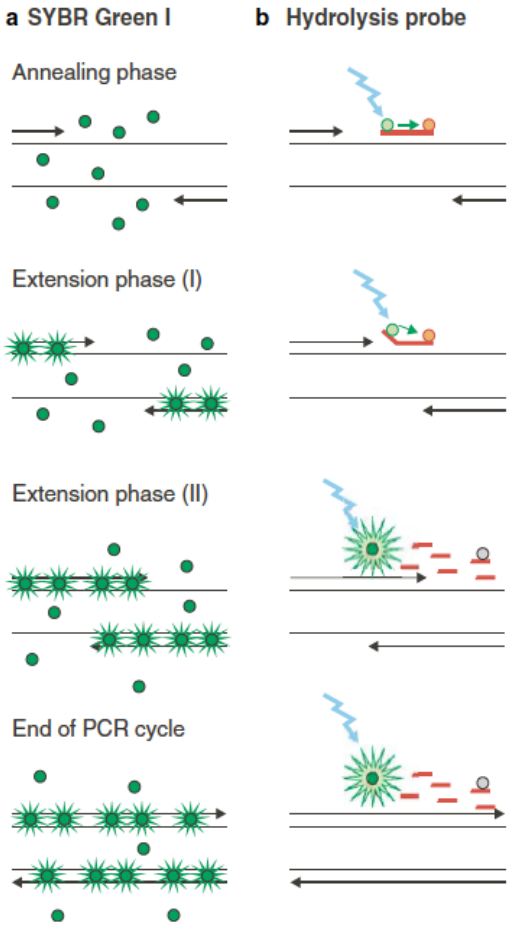

Figure 4.5: This figure demonstrates the principle mechanisms of the SYBR Green dye and the hydrolysis probes, which are used in the TaqMan system.

a) SYBR Green I system. During the elongation phase of the PCR cycle, SYBR Green I dye will bind to dsDNA. If SYBR Green I dye binds the PCR products, fluorescence will be emitted. With each cycle more PCR products will accumulate and with this the detected fluorescence will increase.

b) Hydrolysis probes (TaqMan). The hydrolysis probe holds a quencher fluorochrome on one end and a reporter fluorochrome on the other end. In this close proximity, the quencher absorbs the fluorescence emitted by the reporter. During the elongation phase of the PCR cycle, the hydrolysis probe will be hydrolyzed by the Taq polymerase. This process separates the quencher from the reporter and the fluorescence emitted by the reporter becomes detectable. With each additional PCR cycle, more hydrolysis probes become hydrolyzed as more PCR products are generated. In this way, the fluorescence increases proportionally to the amount of the PCR products. Adapted from V van der Velden, 2003.

4.3.2.2 Basics of real-time PCR evaluation

C_t-values (cycle threshold)

The high accuracy of the real-time PCR is due to the fact that the data are collected during the exponential phase of amplification. This is the phase that is the least susceptible to confounding factors (SM McChlery, 2003). The most important parameter for the evaluation of the data is the threshold cycle. The threshold is a certain fluorescence level, arbitrarily set well above the background fluorescence. The threshold cycle or C_t-value is the cycle when the fluorescence rises above this threshold for the first time.

The C_t-value allows for the comparison of different samples used in one experiment. The higher the initial amount of target DNA, the sooner the fluorescence rises above the threshold. It follows that a small Ct-value corresponds to a higher amount of target sequence in the original cDNA sample and therefore for a higher expression of the gene of interest.

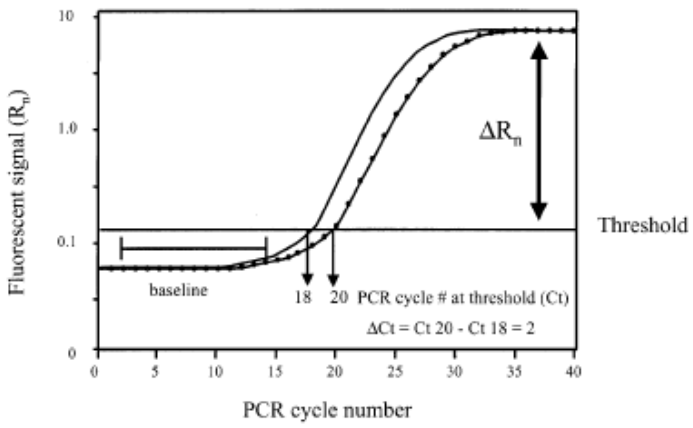

Figure 4.6: This figure displays an example of an amplification plot of a real-time PCR experiment. This hypothetical graph demonstrates important nomenclature for real-time PCR. The plot is achieved by plotting the fluorescence signal versus the PCR cycle number. The baseline describes the range in which the amplification cannot be differentiated from the background fluorescence. The threshold is a line above the background. Fluorescence rising above the threshold is considered as significant and can be used to determine the threshold cycle. The C_t-value is the cycle number in which the plot crosses the threshold. The ΔC_t-value can be calculated by subtracting the C_t-value of one sample from the Ct-value of another sample. A solid line and a dotted line illustrate two different samples. The C_t-value of the solid line is 18, as the line crosses the threshold in this cycle. The C_t -value of the dotted line is 20. Subtracting one from the other, the ΔC_t-value is 2 in this hypothetical case. Adapted from DG Grinzinger, 2002.

Calculation of the efficiency

It is recommended that the efficiency of the PCR amplification is determined before starting the actual experiments (MT Dorak, 2006). Therefore we performed a standard curve analysis. For this, a series of dilutions in 10-fold steps was prepared. Then the C_t-values were plotted against the logarithm of the template concentration. The slope derived from this graph should ideally be about -3.32. This would mean that every target sequence doubles in every cycle. The efficiency (E_x) can be calculated with the slope of the standard curve experiment and Equation 4.1.

$$E_X = 10^{(-1/\text{slope})} - 1$$

Equation 4.1: This equation was used for calculating the efficiency of the primer/probe sets. E_x represents efficiency. The slope is derived from standard curve experiments (MT Dorak, 2006).

We evaluated the efficiency of our PCR on plasmids as well as cDNA of the cell line SEM. The trials with plasmids mostly showed better results than with the cell line. For example, we calculated the efficiency for the primer/probe set OSTL783/883. The experiment with plasmids reached an efficiency of 99%, whereas the experiment using cDNA from the cell line only reached 80% efficiency. The difference in the efficiency could be due to the difference in the amount of target sequence and due to the presence of other transcripts in the cDNA from the SEM cell line. We know that *OSTL* is not expressed in abundance. This becomes apparent in the C_t-value range of the experiments. The experiments with plasmids showed lower C_t-values although we used very high dilutions to ensure a better comparability. But still the plasmid experiment reached C_t-values between 20 and 31, probably due to a greater concentration of the target sequence, whereas the C_t-values of the cell line experiment were in the range of 29 to 37. It is known that the real-time PCR is not as reliable in the higher C_t-value range compared to the lower (MT Dorak, 2006). This could explain the discrepancy between the experiments with the cell line and the plasmids even though the same primer and probe sets were used. And it could be an element of uncertainty in our analysis.

The efficiency varied greatly between different primer/probe sets, although they were all designed using the same standards and most of them reached the same

score in the Primer Express Software. We chose the set with the best efficiency for our experiments, to ensure the best conditions possible. The primer pair OSTL783/883 gave the best results with 99% efficiency in the plasmid standard curve experiment and 80% in the cell line experiment, whereas OSTL861/961 scored slightly inferiorly with 95% and 65%, respectively. OSTL574/647 only reached 39.62% in the plasmid experiment and was excluded. OSTL436/536 showed the worst results with no consistent amplification.

Normalization

To generate valid and objective results, the data obtained from the real-time PCR experiments need to be normalized to so-called control genes. Usually housekeeping genes will be used as endogenous control genes (J Vandesompele, 2002). It is assumed that housekeeping genes are expressed at constant levels in different cell types and throughout the cell cycle.

The internal control system functions as an active reference and is used to compensate for differences in the initial amount of cDNA. Therefore the C_t-value of the control gene is subtracted from the C_t-value of the gene of interest. This results in the ΔC_t-value.

However, there is no guarantee that the housekeeping genes that are expressed at constant levels in healthy cells are also expressed the same way in malignant cells. We evaluated three housekeeping genes: *TBP*, *GUSB* and β-Actin. We chose β-Actin for our experiments, because it showed the most reliable results and Dorak et al. recommend β-Actin for normalization (MT Dorak, 2006).

Comparative C_t-method ($\Delta\Delta C_t$-method)

The comparative C_t-method is used for the relative quantification of the template DNA when the expression level of a given gene should be compared between two samples or two groups of samples. The method is based on the ΔC_t-value (see previous chapter). One group of samples is set as baseline or reference. To achieve the $\Delta\Delta C_t$-value, the ΔC_t-value of the reference will be subtracted from

every sample that it should be compared to. The $\Delta\Delta C_t$-values may be positive or negative (MT Dorak, 2006).

Equation 4.2 can be used to calculate how much the samples differ in expression.

$$\textbf{Fold change} = 2^{-\Delta\Delta Ct}$$

Equation 4.2: With this equation the fold change between two expression levels can be calculated. $\Delta\Delta C_t$ is the difference between the two ΔC_t-values of the two compared values. The equation is based on the assumption that every PCR amplicon doubles in every PCR cycle.

It is assumed that the efficiency is 100%. The standard curve analysis with plasmids showed an efficiency of almost 100%. But this is a rather artificial situation, because in this scenario each plasmid holds the target sequence. The standard curve analysis with the cell line SEM gives a better reflection of the real conditions. Here the efficiency only reached 80%. To take this into account in the calculation, Equation 4.2 needs to be corrected (MW Pfaffl, 2001). This is shown in Equation 4.3. In this way, Equation 4.3 provides more accurate results, which are adapted to the real conditions of the reaction.

$$\textbf{Fold change} = 1.8^{-\Delta\Delta Ct}$$

Equation 4.3: The equation is based on Equation 4.2. It considers the efficiency of 80% of primer/probe set OSTL783/883.

4.4 Conclusion

For this study we used two different methods to analyze the expression profile of *OSTL.* One of the methods, the microarray analysis, has the advantage that it covers a greater collective of patients, as well as a greater variety of leukemia types and even normal bone marrow samples. The other method, the real-time PCR, did not include that many patients but, nevertheless, it is known for its greater specificity and sensitivity.

Despite the methodological differences, the results show the same trend. *OSTL* is expressed higher in CML patients than in other leukemia patients. Additionally the real-time PCR revealed that the expression levels of *OSTL* in the AML cohort do not differ much from the CML patients. This means myeloid leukemia shows the highest expression of *OSTL*. These results were very surprising, because previous experiments indicated that *OSTL* is important for the lymphatic cell lineage.

A hypothesis about how *OSTL* is involved in the development of leukemia is that, because of the dysregulation of *OSTL,* the normal function of HAX-1 or SIVA, or both, are disturbed. This would lead to a disturbance of apoptosis and in this way could contribute to leukemogenesis.

We aimed to gain more information on *OSTL*. Especially we wanted to find a connection between *OSTL* and a leukemia subtype and this way to contribute to the general understanding of *OSTL* in leukemogenesis. The new knowledge of *OSTL* and its potential role in myeloid leukemia may help to establish further experiments that will ultimately have an implication on diagnosis, therapy or prognosis of the patients with CML or AML. For instance it would be interesting to perform a knock-down of *OSTL* in CML cell lines and validate the importance of *OSTL* overexpression for the survival of these cells.

5. Summary

ETV6 is a gene that is known to be involved in translocations, especially in the context of Leukemia. For these translocations several leukemogenic mechanisms have been described. One mechanism is the aberrant or ectopic expression of a neighboring gene. In this way, the focus of interest was directed towards the *OSTL* gene. It is located in direct proximity to the translocation t(6;12)(q23;p13). This translocation involves the *ETV6* gene, as well as a previously unknown gene (named *STL*) and, contrary to expectations, does not produce any functional fusion gene. Therefore L Fontanari Krause analyzed the *OSTL* gene in detail to learn about the leukemogenic potential of this gene, in particular in the context of this translocation.

OSTL is expressed in many different tissues during the embryogenesis of mice, as well as during B-cell development. OSTL protein is highly conserved and little discrepancy can be detected in the protein structure in comparison to the protein in mice. The protein structure of OSTL shows a RING-IBR-RING or TRIAD motive, which is usually found in ubiquitin ligases. Fontanari Krause et al. could not verify this function for the OSTL protein. But they could show an interaction of OSTL with the proteins HAX-1 und SIVA. Both proteins are known to be involved in the regulation of apoptosis.

However, there are still many questions about the concrete function of *OSTL* in the cell as well as its task in leukemogenesis. With this study, we want to approach the question of how *OSTL* could be involved in tumorigenesis. To date it is assumed that the leukemogenic effect of translocations involving *ETV6* is either due to a fusion gene with altered or enhanced function, or to a neighboring gene, which is affected in the way that its expression is changed. In the case of the t(6;12)(q23;p13), no functional fusion gene was found. Therefore we assume that overexpression of *OSTL* is the crucial leukemic effect.

In this study we wanted to find a link of *OSTL* to a certain subgroup of leukemia.

To validate our hypothesis, we used two methods to analyze gene expression. One method (the microarray analysis) provides an overview of the expression levels of many genes in large cohorts of patients. But no precise data of the

expression levels are available with the microarray analysis. To measure the accurate expression levels, we used real-time PCR.

The microarray analysis of 129 patients showed that *OSTL* is expressed approximately twice as high in patients with CML compared to patients with AML, ALL or healthy individuals.

The real-time PCR experiments (39 patients) confirmed the trend in terms of the CML and the ALL cohort. But it appeared that *OSTL* in AML patients is expressed almost equally to the patients with CML. These results show that the expression of *OSTL* is higher in both myeloid leukemias, which is in contrast to our anticipation.

Furthermore, we could demonstrate that *OSTL* is expressed five times lower in ALL patients than in the patients with myeloid leukemia. The ALL cohort is very heterogeneous and we could show that in the ALL-Ph+ subgroup, *OSTL* is expressed nine times lower than in the CML patients, whereas in the T-ALL group it is expressed only 1.5 times lower.

In summary, our results demonstrate that overexpression of *OSTL* is rather linked to myeloid leukemia and not, as expected, to lymphoid leukemia. These results provide novel information that might be the basis for experiments that answer questions concerning the leukemogenic effect of *OSTL*.

6. Zusammenfassung

In der aktuellen Forschung wird Translokationen ein immer höherer Stellenwert in der Entstehung von Leukämien zugemessen. Das Gen *ETV6* wurde als häufiger Translokationspartner identifiziert und verschiedene leukämogene Mechanismen dieser Translokationen sind bisher beschrieben worden. Einer dieser Mechanismen beinhaltet, dass es durch die Translokation zu einer ektopen oder aberranten Expression von benachbarten Genen kommt. So ist man auf das Gen *OSTL* aufmerksam geworden. Es liegt in der unmittelbaren Nähe der Translokation t(6;12)(q23;p13), welche das Gen *ETV6* sowie ein zuvor unbekanntes Gen (*STL*) betrifft und zu keinem funktionsfähigen Fusionsgen führt. Fontanari Krause et al. haben daraufhin das Gen *OSTL* eingehend charakterisiert.

Das Gen *OSTL* wird während der Embryogenese der Maus in vielen Geweben sowie während der B-Zell-Entwicklung exprimiert. *OSTL* ist hoch konserviert und es wurden nur geringe Abweichungen in der Protein-Struktur im Vergleich zum Maus-Protein gefunden. Auf Proteinebene zeigte sich ein RING-IBR-RING beziehungsweise ein TRIAD-Motiv, welches normalerweise für Ubiquitinligasen typisch ist. Diese Funktion konnte bei dem Protein OSTL nicht nachgewiesen werden. Allerdings zeigten Experimente eine Interaktion mit den Proteinen HAX-1 und SIVA, die beide in die Regulation von Apoptosen involviert sind.

Es sind jedoch noch viele Fragen hinsichtlich der genauen Funktion von OSTL in der Zelle und bezüglich des Einflusses auf die Leukämieentstehung offen. Bisher wird angenommen, dass es sich bei dem leukämogenen Effekt von Translokationen mit *ETV6* entweder um ein Fusionsgen mit veränderter beziehungsweise verstärkter Funktion handelt oder um ein benachbartes Gen, das durch die Translokation sein Expressionsverhalten ändert. Da im Fall der t(6;12)(q23;p13) kein funktionsfähiges Fusionsgen gefunden wurde, gehen wir davon aus, dass es sich hier um den anderen Mechanismus handeln muss.

Um diese Hypothese zu bestätigen haben wir uns zweier Methoden zur Analyse von Genexpression bedient. Die Microarray-Methode gibt einen Überblick über die Expression einer Vielzahl von Genen und hat in diesem Fall den Vorteil, dass mit dieser Methode ein größeres Patientenkollektiv erfasst wurde. Die Microarray-

Analyse gibt aber keine genauen Angaben über die Expressionshöhe. Um jedoch auch die exakten Expressionslevel von *OSTL* zu erfahren, haben wir zusätzlich real-time PCR-Experimente durchgeführt.

Dabei haben wir eine erhöhte Expression von *OSTL* in der Gruppe der Patienten mit ALL erwartet, da die Translokation bei einem Patienten mit B-Zell ALL entdeckt wurde und da *OSTL* in vorangegangenen Experimenten eher mit dem lymphatischen System in Verbindung gebracht wurde.

Mit dieser Arbeit wollten wir eine Verbindung von *OSTL* zu einer Untergruppe der Leukämien finden.

In der Microarray-Analyse von 129 Patienten zeigte sich, dass *OSTL* ungefähr doppelt so hoch bei Patienten mit CML exprimiert wird wie bei Patienten mit AML, ALL oder nicht erkrankten Patienten.

Die real-time PCR-Experimente (39 Patienten) haben den gleichen Trend gezeigt wie die Microarray-Analyse. CML zeigt auch hier die höchste Expression. Es stellte sich jedoch heraus, dass *OSTL* bei AML Patienten nahezu gleich wie bei CML Patienten exprimiert wird. Dies bedeutet, dass *OSTL* am höchsten in den myeloischen Leukämien exprimiert wird. Diese Ergebnisse weichen von der Ausgangshypothese ab.

Außerdem konnte gezeigt werden, dass die Expression von *OSTL* bei ALL Patienten fast fünffach geringer ausgeprägt ist gegenüber den Patienten mit myeloischen Leukämien. Allerdings variiert das Expressionsverhalten unter den ALL-Subgruppen erheblich, genauer zwischen einer neunfach geringeren Expression im Vergleich zu den myeloischen Leukämien in der ALL-Ph+ Gruppe und einer nur 1,5-fach geringeren Expression in der T-ALL Kohorte.

Zusammenfassend handelt es sich um überraschende Ergebnisse, die *OSTL*-Überexpression mit myeloischen und nicht wie erwartet mit lymphatischen Leukämien in Verbindung bringen. Diese neuen Informationen über *OSTL* stellen eine Grundlage für weitere Experimente dar, welche zum Verständnis der Entstehung von Leukämien beitragen können.

7. References

Aplan PD. Causes of oncogenic chromosomal translocation. Trends Genet. 2006 Jan;22(1):46-55. Epub 2005 Oct 28.

Babu MM. Introduction to microarray data analysis. Computational Genomics (Ed: R. Grant), Horizon Press, U.K.

Barkinge JL, Gudi R, Sarah H, Chu F, Borthakur A, Prabhakar BS, Prasad KV. The p53-induced Siva-1 plays a significant role in cisplatin-mediated apoptosis. J Carcinog. 2009;8:2.

Ben-Bassat H, Goldblum N, Mitrani S, Goldblum T, Yoffey JM, Cohen MM, Bentwich Z, Ramot B, Klein E, Klein G Establishment in continuous culture of a new type of lymphocyte from a "Burkitt like" malignant lymphoma (line D.G.-75). Int J Cancer. 1977 Jan;19(1):27-33.

Beverloo HB, Panagopoulos I, Isaksson M, van Wering E, van Drunen E, de Klein A, Johansson B, Slater R. Fusion of the homeobox gene HLXB9 and the ETV6 gene in infant acute myeloid leukemias with the t(7;12)(q36;p13). Cancer Res. 2001 Jul 15;61(14):5374-7.

Bohlander SK. Fusion genes in leukemia: an emerging network. Cytogenet Cell Genet. 2000; 91(1-4):52-6.

Bohlander SK. ETV6: a versatile player in leukemogenesis. Semin Cancer Biol. 2005 Jun;15(3):162-74.

Buijs A, van Rompaey L, Molijn AC, Davis JN, Vertegaal AC, Potter MD, Adams C, van Baal S, Zwarthoff EC, Roussel MF, Grosveld GC. The MN1-TEL fusion protein, encoded by the translocation (12;22)(p13;q11) in myeloid leukemia, is a transcription factor with transforming activity. Mol Cell Biol. 2000 Dec;20(24):9281-93.

Burmeister T, Thiel E. Molecular genetics in acute and chronic leukemias. J Cancer Res Clin Oncol. 2001 Feb;127(2):80-90.

Capili AD, Edghill EL, Wu K, Borden KL. Structure of the C-terminal RING finger from a RING-IBR-RING/TRIAD motif reveals a novel zinc-binding domain distinct from a RING. J Mol Biol. 2004 Jul 23;340(5):1117-29.

Chen Y, Gelfond JA, McManus LM, Shireman PK. Reproducibility of quantitative RT-PCR array in miRNA expression profiling and comparison with microarray analysis. BMC Genomics. 2009 Aug 28;10:407.

Chase A, Reiter A, Burci L, Cazzaniga G, Biondi A, Pickard J, Roberts IA, Goldman JM, Cross NC. Fusion of ETV6 to the caudal-related homeobox gene CDX2 in acute myeloid leukemia with the t(12;13)(p13;q12). Blood. 1999 Feb 1;93(3):1025-31.

Cools J, Bilhou-Nabera C, Wlodarska I, Cabrol C, Talmant P, Bernard P, Hagemeijer A, Marynen P. Fusion of a novel gene, BTL, to ETV6 in acute myeloid leukemias with a t(4;12)(q11-q12;p13). Blood. 1999 Sep 1;94(5):1820-4.

Cools J, Mentens N, Odero MD, Peeters P, Wlodarska I, Delforge M, Hagemeijer A, Marynen P. Evidence for position effects as a variant ETV6-mediated leukemogenic mechanism in myeloid leukemias with a t(4;12)(q11-q12;p13) or t(5;12)(q31;p13). Blood. 2002 Mar 1;99(5):1776-84.

Cornell RF, Palmer J. Adult acute leukemia. Dis Mon. 2012 Apr;58(4):219-38.

Cortes J, Kantarjian H. How I treat newly diagnosed chronic phase CML. Blood. 2012 Aug 16;120(7):1390-7.

de Klein A, van Kessel AG, Grosveld G, Bartram CR, Hagemeijer A, Bootsma D, Spurr NK, Heisterkamp N, Groffen J, Stephenson JR. A cellular oncogene is translocated to the Philadelphia chromosome in chronic myelocytic leukaemia. Nature. 1982 Dec 23;300(5894):765-7.

Dorak MT (Ed): Real-Time PCR (Advanced Methods Series). Oxford: Taylor & Francis, 2006.

Eguchi-Ishimae M, Eguchi M, Maki K, Porcher C, Shimizu R, Yamamoto M, Mitani K. Leukemia-related transcription factor TEL/ETV6 expands erythroid precursors and stimulates hemoglobin synthesis. Cancer Sci. 2009 Apr;100(4):689-97. Epub 2009.

Fenrick R, Amann JM, Lutterbach B, Wang L, Westendorf JJ, Downing JR, Hiebert SW. Both TEL and AML-1 contribute repression domains to the t(12;21) fusion protein. Mol Cell Biol. 1999 Oct;19(10):6566-74.

Fontanari Krause L. Identification and functional characterization of the human and murine OSTL gene, which encodes a RING-DRIL-RING domain protein possibly involved in B cell differentiation and leukemogenesis. Dissertation; LMU Munich, Department of Biology. 2006.

Golub TR, Barker GF, Lovett M, Gilliland DG. Fusion of PDGF receptor beta to a novel ets-like gene, tel, in chronic myelomonocytic leukemia with t(5;12) chromosomal translocation. Cell. 1994 Apr 22;77(2):307-16.

Greil J, Gramatzki M, Burger R, Marschalek R, Peltner M, Trautmann U, Hansen-Hagge TE, Bartram CR, Fey GH, Stehr K, et al. The acute lymphoblastic leukaemia cell line SEM with t(4;11) chromosomal rearrangement is biphenotypic and responsive to interleukin-7. Br J Haematol. 1994 Feb;86(2):275-83.

Grimshaw SJ, Mott HR, Stott KM, Nielsen PR, Evetts KA, Hopkins LJ, Nietlispach D, Owen D. Structure of the sterile alpha motif (SAM) domain of the Saccharomyces cerevisiae mitogen-activated protein kinase pathway-modulating protein STE50 and analysis of its interaction with the STE11 SAM. J Biol Chem. 2004 Jan 16;279(3):2192-201. Epub 2003 Oct 22.

Ginzinger DG. Gene quantification using real-time quantitative PCR: an emerging technology hits the mainstream. Exp Hematol. 2002 Jun;30(6):503-12.

Gudi R, Barkinge J, Hawkins S, Chu F, Manicassamy S, Sun Z, Duke-Cohan JS, Prasad KV. Siva-1 negatively regulates NF-kappaB activity: effect on T-cell receptor-mediated activation-induced cell death (AICD). Oncogene. 2006 Jun 8;25(24):3458-62. Epub 2006 Feb 20.

Han Y, Chen YS, Liu Z, Bodyak N, Rigor D, Bisping E, Pu WT, Kang PM. Overexpression of HAX-1 protects cardiac myocytes from apoptosis through caspase-9 inhibition. Circ Res. 2006 Aug 18;99(4):415-23. Epub 2006 Jul 20.

Harris NL, Jaffe ES, Diebold J, Flandrin G, Muller-Hermelink HK, Vardiman J, Lister TA, Bloomfield CD. The World Health Organization classification of neoplasms of the hematopoietic and lymphoid tissues: report of the Clinical Advisory Committee meeting--Airlie House, Virginia, November, 1997. Hematol J. 2000;1(1):53-66.

Hayashi Y, Raimondi SC, Look AT, Behm FG, Kitchingman GR, Pui CH, Rivera GK, Williams DL. Abnormalities of the long arm of chromosome 6 in childhood acute lymphoblastic leukemia. Blood. 1990 Oct 15;76(8):1626-30.

Hecht JL, Aster JC. Molecular biology of Burkitt's lymphoma. J Clin Oncol. 2000 Nov 1;18(21):3707-21.

Heisterkamp N, Stam K, Groffen J, de Klein A, Grosveld G. Structural organization of the bcr gene and its role in the Ph' translocation. Nature. 1985 Jun 27-Jul 3;315(6022):758-61.

Hiebert SW, Sun W, Davis JN, Golub T, Shurtleff S, Buijs A, Downing JR, Grosveld G, Roussell MF, Gilliland DG, Lenny N, Meyers S. The t(12;21) translocation converts AML-1B from an activator to a repressor of transcription. Mol Cell Biol. 1996 Apr;16(4):1349-55.

Hock H, Meade E, Medeiros S, Schindler JW, Valk PJ, Fujiwara Y, Orkin SH. Tel/Etv6 is an essential and selective regulator of adult hematopoietic stem cell survival.Genes Dev. 2004 Oct 1;18(19):2336-41. Epub 2004 Sep 15.

Huber W, von Heydebreck A, Sültmann H, Poustka A, Vingron M. Variance stabilization applied to microarray data calibration and to the quantification of differential expression. Bioinformatics. 2002;18 Suppl 1:S96-104.

Johansson B, Mertens F, Mitelman F. Clinical and biological importance of cytogenetic abnormalities in childhood and adult acute lymphoblastic leukemia. Annals of Medicine. 2004; 36, 492–503.

Kennedy JA, Barabé F. Investigating human leukemogenesis: from cell lines to in vivo models of human leukemia. Leukemia. 2008 Nov;22(11):2029-40. Epub 2008 Aug 7.

Klein C, Grudzien M, Appaswamy G, Germeshausen M, Sandrock I, Schäffer AA, Rathinam C, Boztug K, Schwinzer B, Rezaei N, Bohn G, Melin M, Carlsson G, Fadeel B, Dahl N, Palmblad J, Henter JI, Zeidler C, Grimbacher B, Welte K. HAX1 deficiency causes autosomal recessive severe congenital neutropenia (Kostmann disease). Nat Genet. 2007 Jan;39(1):86-92. Epub 2006 Dec 24.

Klug WS, Cummings MR, Spencer CA. Concepts of Genetics. Prentice Hall. 2005.

Knudson AG Jr. Mutation and cancer: statistical study of retinoblastoma. Proc Natl Acad Sci U S A. 1971 Apr;68(4):820-3.

Kobayashi H, Montgomery KT, Bohlander SK, Adra CN, Lim BL, Kucherlapati RS, Donis-Keller H, Holt MS, Le Beau MM, Rowley JD. Fluorescence in situ hybridization mapping of translocations and deletions involving the short arm of human chromosome 12 in malignant hematologic diseases. Blood. 1994 Nov 15;84(10): 3473-82.

Krug U, Ganser A, Koeffler HP. Tumor suppressor genes in normal and malignant hematopoiesis. Oncogene. 2002 May 13;21(21):3475-95.

Lodish H, Berk A, Matsudaira P, Kaiser CA, Krieger M, Scott MA, Zipursky L, Darnell J. Molecular Cell Biology. W.H. Freeman & Company. 2007.

Marschalek R, Greil J, Löchner K, Nilson I, Siegler G, Zweckbronner I, Beck JD, Fey GH.Molecular analysis of the chromosomal breakpoint and fusion transcripts in the acute lymphoblastic SEM cell line with chromosomal translocation t(4;11). Br J Haematol. 1995 Jun;90(2):308-20.

Mathers CD, Boschi-Pinto C, Lopez AD, Murray CJL. Cancer incidence, mortality and survival by site for 14 regions of the world. 2001. Global Programme on Evidence for Health Policy Discussion Paper No. 13 (World Health Organization).

McKenna RW. Multifaceted approach to the diagnosis and classification of acute leukemias. Clin Chem. 2000 Aug;46(8 Pt 2):1252-9.

Mirmohammadsadegh A, Tartler U, Michel G, Baer A, Walz M, Wolf R, Ruzicka T, Hengge UR. HAX-1, identified by differential display reverse transcription polymerase chain reaction, is overexpressed in lesional psoriasis. J Invest Dermatol. 2003 Jun;120(6):1045-51.

McChlery SM, Clarke SC. The use of hydrolysis and hairpin probes in real-time PCR. Mol Biotechnol. 2003 Nov;25(3):267-74.

Mitelman F, Johansson B, Mertens F. The impact of translocations and gene fusions on cancer causation. Nat Rev Cancer 2007; vol. 7:233–245.

Mu Q, Cheng Y, Xu W, Wang Y, Chen Z, Jin J. Acquired Robertsonian translocation is not always suggestive of poor prognosis: a case of acquired Rob(13;14) in Philadelphia chromosome-negative cells of chronic myelogenous leukemia. Leuk Lymphoma. 2010 Nov;51(11):2141-3. Epub 2010 Sep 21.

Nambiar M, Kari V, Raghavan SC. Chromosomal translocations in cancer. Biochim Biophys Acta. 2008 Dec;1786(2):139-52. Epub 2008 Jul 31.

Nygaard V, Løland A, Holden M, Langaas M, Rue H, Liu F, Myklebost O, Fodstad Ø, Hovig E, Smith-Sørensen B. Effects of mRNA amplification on gene expression ratios in cDNA experiments estimated by analysis of variance. BMC Genomics. 2003 Mar 23;4(1):11. Epub 2003 Mar 23.

Odero MD, Vizmanos JL, Román JP, Lahortiga I, Panizo C, Calasanz MJ, Zeleznik-Le NJ, Rowley JD, Novo FJ. A novel gene, MDS2, is fused to ETV6/TEL in a t(1;12)(p36.1;p13) in a patient with myelodysplastic syndrome. Genes Chromosomes Cancer. 2002 Sep;35(1):11-9.

Oikawa T, Yamada T. Molecular biology of the Ets family of transcription factors. Gene. 2003 Jan 16;303:11-34.

Okuno K, Yasutomi M, Nishimura N, Arakawa T, Shiomi M, Hida J, Ueda K, Minami K. Gene expression analysis in colorectal cancer using practical DNA array filter. Dis Colon Rectum. 2001 Feb;44(2):295-9.

Panagopoulos I, Strömbeck B, Isaksson M, Heldrup J, Olofsson T, Johansson B. Fusion of ETV6 with an intronic sequence of the BAZ2A gene in a paediatric pre-B acute lymphoblastic leukaemia with a cryptic chromosome 12 rearrangement. Br J Haematol. 2006 May;133(3):270-5.

Pfaffl MW. A new mathematical model for relative quantification in real-time RT-PCR. Nucleic Acids Res. 2001 May 1;29(9):e45.

Prasad KV, Ao Z, Yoon Y, Wu MX, Rizk M, Jacquot S, Schlossman SF. CD27, a member of the tumor necrosis factor receptor family, induces apoptosis and binds to Siva, a proapoptotic protein. Proc Natl Acad Sci U S A. 1997 Jun 10;94(12):6346-51.

Ramiro AR, Jankovic M, Callen E, Difilippantonio S, Chen HT, McBride KM, Eisenreich TR, Chen J, Dickins RA, Lowe SW, Nussenzweig A, Nussenzweig MC. Role of genomic instability and p53 in AID-induced c-myc-Igh translocations. Nature. 2006 Mar 2;440(7080):105-9. Epub 2006 Jan 8.

Rabbitts TH. Chromosomal translocations in human cancer. Nature. 1994 Nov 10;372(6502):143-9.

Rawat VPS, Cusan M, Deshpande A, Hiddemann W, Quintanilla-Martinez L, Humphries RK, Bohlander SK, Feuring-Buske M, Buske C. Ectopic expression of the homeobox gene Cdx2 is the transforming event in a mouse model of t(12;13)(p13;q12) acute myeloid leukemia. Proc Natl Acad Sci U S A. 2004 Jan 20;101(3):817-22

Rawat VP, Thoene S, Naidu VM, Arseni N, Heilmeier B, Metzeler K, Petropoulos K, Deshpande A, Quintanilla-Martinez L, Bohlander SK, Spiekermann K, Hiddemann W, Feuring-Buske M, Buske C. Overexpression of CDX2 perturbs HOX gene expression in murine progenitors depending on its N-terminal domain and is closely correlated with deregulated HOX gene expression in human acute myeloid leukemia. Blood. 2008 Jan 1;111(1):309-19. Epub 2007 Sep 12.

Ririe KM, Rasmussen RP, Wittwer CT. Product differentiation by analysis of DNA melting curves during the polymerase chain reaction. Anal Biochem. 1997 Feb 15;245(2):154-60.

Rowley JD. The role of chromosome translocations in leukemogenesis. Semin Hematol. 1999 Oct;36(4 Suppl 7):59-72.

Schäffer AA, Klein C. Genetic heterogeneity in severe congenital neutropenia: how many aberrant pathways can kill a neutrophil? Curr Opin Allergy Clin Immunol. 2007 Dec;7(6):481-94.

Schena M, Shalon D, Davis RW, Brown PO. Quantitative monitoring of gene expression patterns with a complementary DNA microarray. Science. 1995 Oct 20;270(5235):467-70.

Schoch C, Kohlmann A, Schnittger S, Brors B, Dugas M, Mergenthaler S, Kern W, Hiddemann W, Eils R, Haferlach T. Acute myeloid leukemias with reciprocal rearrangements can be distinguished by specific gene expression profiles. Proc Natl Acad Sci U S A. 2002 Jul 23;99(15):10008-13. Epub 2002 Jul 8.

Scholl C, Bansal D, Döhner K, Eiwen K, Huntly BJ, Lee BH, Rücker FG, Schlenk RF, Bullinger L, Döhner H, Gilliland DG, Fröhling S. The homeobox gene CDX2 is aberrantly expressed in most cases of acute myeloid leukemia and promotes leukemogenesis. J Clin Invest. 2007 Apr;117(4):1037-48.

Sharrocks AD. The ETS-domain transcription factor family. Nat Rev Mol Cell Biol. 2001 Nov;2(11):827-37.

Shaw J, Kirshenbaum LA. HAX-1 represses postmitochondrial caspase-9 activation and cell death during hypoxia-reoxygenation. Circ Res. 2006 Aug 18;99(4):336-8

Shurtleff SA, Buijs A, Behm FG, Rubnitz JE, Raimondi SC, Hancock ML, et al. Tel/AML1 fusion resulting from a cryptic t(12;21) is the most common genetic lesion in pediatric ALL and defines a subgroup of patients with an excellent prognosis. Leukemia 1995;9:1985–9.

Slupsky CM, Gentile LN, Donaldson LW, Mackereth CD, Seidel JJ, Graves BJ, McIntosh LP. Structure of the Ets-1 pointed domain and mitogen-activated protein kinase phosphorylation site. Proc Natl Acad Sci U S A. 1998 Oct 13;95(21):12129-34.

Suto Y, Sato Y, Smith SD, Rowley JD, Bohlander SK. A t(6;12)(q23;p13) results in the fusion of ETV6 to a novel gene, STL, in a B-cell ALL cell line. Genes Chromosomes Cancer. 1997 Apr;18(4):254-68.

Suzuki Y, Demoliere C, Kitamura D, Takeshita H, Deuschle U, Watanabe T. HAX-1, a novel intracellular protein, localized on mitochondria, directly associates with HS1, a substrate of Src family tyrosine kinases. J Immunol. 1997 Mar 15;158(6):2736-44.

Swerdlow SH, Campo E, Harris NL, Jaffe ES, Pilleri SA, Stein H, et al, eds. WHO classification of tumours of haematopoietic and lymphoid tissues. 4th ed. IARC Press, 2008.

Thoene S, Rawat VP, Heilmeier B, Hoster E, Metzeler KH, Herold T, Hiddemann W, Gökbuget N, Hoelzer D, Bohlander SK, Feuring-Buske M, Buske C. The homeobox gene CDX2 is aberrantly expressed and associated with an inferior prognosis in patients with acute lymphoblastic leukemia. Leukemia. 2009 Apr;23(4):649-55. Epub 2009 Jan 22.

Turner SD, Alexander DR. Fusion tyrosine kinase mediated signalling pathways in the transformation of haematopoietic cells. Leukemia. 2006 Apr;20(4):572-82.

Vardiman JW, Harris NL, Brunning RD. The World Health Organization (WHO) classification of the myeloid neoplasms. Blood. 2002 Oct 1;100(7):2292-302.

Vardiman JW, Thiele J, Arber DA, Brunning RD, Borowitz MJ, Porwit A, Harris NL, Le Beau MM, Hellström-Lindberg E, Tefferi A, Bloomfield CD. The 2008 revision of the World Health Organization (WHO) classification of myeloid neoplasms and acute leukemia: rationale and important changes. Blood. 2009 Jul 30;114(5):937-51. Epub 2009 Apr 8.

Wang LC, Kuo F, Fujiwara Y, Gilliland DG, Golub TR, Orkin SH., Yolk sac angiogenic defect and intra-embryonic apoptosis in mice lacking the Ets-related factor TEL. EMBO J. 1997 Jul 16;16(14):4374-83.

Wang LC, Swat W, Fujiwara Y, Davidson L, Visvader J, Kuo F, Alt FW, Gilliland DG, Golub TR, Orkin SH., The TEL/ETV6 gene is required specifically for hematopoiesis in the bone marrow. Genes Dev. 1998 Aug 1;12(15):2392-402.

Warner JK, Wang JC, Hope KJ, Jin L, Dick JE. Concepts of human leukemic development. Oncogene. 2004 Sep 20;23(43):7164-77.

Wasylyk B, Hahn SL, Giovane A. The Ets family of transcription factors. Eur J Biochem. 1993 Jan 15;211(1-2):7-18.

van Haaften RI, Schroen B, Janssen BJ, van Erk A, Debets JJ, Smeets HJ, Smits JF, van den Wijngaard A, Pinto YM, Evelo CT. Biologically relevant effects of mRNA amplification on gene expression profiles. BMC Bioinformatics. 2006 Apr 11;7:200.

van der Velden VH, Hochhaus A, Cazzaniga G, Szczepanski T, Gabert J, van Dongen JJ. Detection of minimal residual disease in hematologic malignancies by real-time quantitative PCR: principles, approaches, and laboratory aspects. Leukemia. 2003 Jun;17(6):1013-34.

van Wely KH, Molijn AC, Buijs A, Meester-Smoor MA, Aarnoudse AJ, Hellemons A, den Besten P, Grosveld GC, Zwarthoff EC. The MN1 oncoprotein synergizes with coactivators RAC3 and p300 in RAR-RXR-mediated transcription.Oncogene. 2003 Feb 6;22(5):699-709.

van Wely KH, Meester-Smoor MA, Janssen MJ, Aarnoudse AJ, Grosveld GC, Zwarthoff EC. The MN1-TEL myeloid leukemia-associated fusion protein has a dominant-negative effect on RAR-RXR-mediated transcription. Oncogene. 2007 Aug 23;26(39):5733-40. Epub 2007 Mar 19.

Vandesompele J, De Preter K, Pattyn F, Poppe B, Van Roy N, De Paepe A, Speleman F. Accurate normalization of real-time quantitative RT-PCR data by geometric averaging of multiple internal control genes. Genome Biol. 2002 Jun 18;3(7):RESEARCH0034. Epub 2002 Jun 18.

Wheatley K, Burnett AK, Goldstone AH, Gray RG, Hann IM, Harrison CJ, Rees JK, Stevens RF, Walker H. A simple, robust, validated and highly predictive index for the determination of risk-directed therapy in acute myeloid leukaemia derived from the MRC AML 10 trial. United Kingdom Medical Research Council's Adult and Childhood Leukaemia Working Parties. Br J Haematol. 1999 Oct;107(1):69-79.

Yamamoto JF, Goodman MT. Patterns of leukemia incidence in the United States by subtype and demographic characteristics, 1997-2002. Cancer Causes Control. 2008 May;19(4):379-90. Epub 2007 Dec 7.

Zhang LQ, Downie PA, Goodell WR, McCabe NR, LeBeau MM, Morgan R, Sklar J, Raimondi SC, Miley D, Goldberg A, et al. Establishment of cell lines from B-cell precursor acute lymphoblastic leukemia. Leukemia. 1993 Nov;7(11):1865-74.

Appendix: Table with patient details

No	Type of Leukemia	Age at diagnosis	Karyotype	Molecular Marker
1	CML	72	46,XX,t(9;22)(q34;q11) [24] 46,XX [1]	BCR-ABL- fusion transcript type b2a2
2	CML	51	46,XY,t(9;22)(q34;q11) [25]	BCR-ABL- fusion transcript type b3a2
3	CML	63	46,XY,t(9;22)(q34;q11) [25]	BCR-ABL- fusion transcript type b2a2
4	CML	44	46,XX,t(9;22)(q34;q11) [25]	BCR-ABL- fusion transcript type b2a2
5	CML	59	46,XX,t(9;22)(q34;q11) [25]	BCR-ABL- fusion transcript type b3a2
6	CML	73	46,XY,t(9;22)(q34;q11) [25]	BCR-ABL- fusion transcript type b3a2
7	CML	61	46,XX,t(9;22)(q34;q11) [25]	BCR-ABL- fusion transcript type b3b2a2
8	CML	35	46,XY,t(9;22)(q34;q11) [25]	BCR-ABL- fusion transcript type b3a2
9	CML	47	46,XX,t(9;22)(q34;q11) [25]	BCR-ABL- fusion transcript type b3a2
10	CML	64	46,XY,t(9;22)(q34;q11) [25]	BCR-ABL- fusion transcript type b2a2
11	ALL; Ph pos	66	46,XY,t(9;22)(q34;q11),del(9)(p22) [10] 46,XY [13]	BCR-ABL- fusion transcript
12	ALL; Ph pos	62	46,XX,der(9)t(9;22)(q34;q11)del(9)(p13),der(19)t(8;19)(q13;p13),der(22), t(9;22)(q34;q11) [13] 46,XX [5]	BCR-ABL- fusion transcript
13	ALL; Ph pos	74	47,XY,t(2;16)(p11;p11),+8, t(9;22)(q34;q11) [14] 46,XY [6]	BCR-ABL- fusion transcript type e1a3

14	ALL; Ph pos	39	45,XY,der(7;9)(q10;q10), t(9;22)(q34;q11) [6] 46,XY [16]	BCR-ABL-fusion transcript type b2a2
15	ALL; Ph pos	39	45,XY,-9,t(9;22)(q34;q11)[3] 46,XY,idem,+der(22)t(9;22)(q34;q11) [22]	BCR-ABL-fusion transcript type; second time no detection
16	ALL; t4;11pos	37	46,XY,t(4;11)(q21;q23) [17] 46,XY [3]	MLL-AF4 pos FLT3D324- FLT3V592-
17	ALL; t4;11pos	61	46,XX,t(4;11)(q21;q23) [5]	FLT3-LM- MLL-AF4+
18	ALL; t4;11pos	71	46,XX,t(4;11)(q21;q23)[14] 46,XX [3]	MLL-AF4+
19	ALL; t4;11pos	25	46,XX,t(4;11)(q21;q23)[18] 46,XX [1]	MLL-AF4+
20	ALL; t4;11pos	68	46,XX,t(4;11)(q21;q23)[4]	MLL-AF4+ FLT3-LM-
21	common ALL	37	81-86,XX,-X,-X,del(1)(p32),-2, -4,+5,t(5;11)(?;?),-6,-7,+8,-10,-11,-12,-15,-17 [cp5] 46,XX [13]	FLT3D324-
22	common ALL	21	46-47,XX, del(6)(q15),der(8)t(8;15)(p11;q11), ins(12;21)(p13;q22q22),-15,+16 [cp10]	
23	common ALL	72	47,XX,+X [1] 47,XX,+X,i(8)(q10)[1],46,XX [18]	FLT3-LM-
24	common ALL	79	62-64,XXY,+Y,-2,-3,+6,-7,+8,-9,+11,+12, -13,-15,der(15;18)(q10;q10),-16,-17, -18,+19,der(19)t(6;19)(q11;p13) [cp6] 46,XY [14]	
25	common ALL	77	46,XX,t(X;14)(p22.3;q32) [10] 46,XX [10]	
26	T-ALL	19	46,XX,del(7)(q22) [12] 46,XX [9]	
27	T-ALL	59	4- 45,XX,der(1)t(1;18),del(3)(p?),del(4) (q11),der(5)t(4;5)(?;q11),del(9)(q11), del(11)(q11),der(13)t(11;13)t(11;16), der(19)t(1;19)t(1;4),der(21)t(16;21) [cp11] 88-90,idemx2 [cp2] 46,XX [2]	NPM1- FLT3-LM-

28	T-ALL	33	48,XY,+8,del(9)(p13p22),+10 [9] 46,XY [10]	FLT3-LM- NPM1-
29	T-ALL	64	46,XY,der(2;17)(p11;q11),del(7)(q11.2), der(16)t(7;16)(?;q22)t(2;7)(p11;?),der(17)del(17)(p11)del(17)(q12) [14] 46,XY [1]	
30	T-ALL	n/a	46,XY,del(9)(p?13p?23), +del(9)(p?13p?23),der(10;21)(q10;q10) [8] 46,XY [6]	
31	AML norm karyotype	21	46,XY	NPM1+ FLT3-LM-
32	AML norm karyotype	37	46,XY	FLT3-LM- NPM1+ NRAS codon 12+
33	AML norm karyotype	68	46,XY	FLT3- NPM1-
34	AML norm karyotype	42	46,XX	FLT3+ FLT3-LM+ NPM1+
35	AML norm karyotype	63	46,XY	FLT3- NPM1+
36	AML norm karyotype	66	46,XX	FLT3-LM- NPM1- CEBPA+
37	AML norm karyotype	72	46,XX	FLT3-LM- NPM1-
38	AML norm karyotype	63	46,XX	FLT3-LM- NPM1+ FLT3D835+
39	AML norm karyotype	70	46,XY	FLT3-LM+ NPM1-
40	AML norm karyotype	79	46,XX	RNA FLT3-LM- NPM1+

Abbreviations

°C	Degree Celsius
AA = aa	Amino acids
AICD	Activation-induced cell death
ALL	Acute Lymphoid/Lymphoblastic Leukemia
AML	Acute Myeloid/Myelogenous Leukemia
Aqua bidest.	Water double deionized filtered trough Millipore filters
BLAST	Basic Local Alignment Search Tool
BM	Bone Marrow
B-NHL	B-cell-Non-Hodgkin-Lymphoma
bp	Base pair(s)
C	Cytosine
cDNA	Complementary DNA, synthetic DNA transcribed from a specific RNA through the action of the reverse transcriptase
CML	Chronic Myeloid/Myelogenous Leukemia
C_t	Threshold cycle
ΔC_t	C_t-value normalized with the C_t-value of a housekeeping gene
$\Delta\Delta C_t$	Difference between 2 ΔC_t-values of interest
del	Deletion
DEPC	Diethyl pyrocarbonate

DMEM	Dulbecco’s Modified Eagle Medium
DMSO	Dimethylsulfoxide
DNA	Deoxyribonucleic acid
DNase	Desoxyribonuklease
DRIL	Double RING finger linked
dNTP	Deoxynucleotidetriphosphate
dsDNA	Double-stranded DNA
DSMZ	German Collection of Microorganisms and Cell Cultures
DTT	Dithiothreitol
EBV	Epstein–Barr virus
EDTA	Ethylenediaminetetraacetic acid
E_x	Efficiency of the real time PCR reaction
FAB	French-American-British Classification
FCS	Fetal calf serum
FISH	Fluorescence-in-situ-hybridization
FRET	Förster (fluorescence) resonance energy transfer
FW	Forward
g	Gram
G	Guanine
HLH	Helix loop helix
HSC	Hematopoietic stem cell
IBR	In between RING fingers
Ig	Immunoglobulin

IgH	Immunoglobulin; heavy chain
IgL	Immunoglobulin; light chain
Inv	Inversion
IQR	inter quantile range
l	Liter
M	Molar
MDS	Myelodysplastic Syndrome
µg	Microgram
min	Minute(s)
mix	Mixture
ml	Milliliter
µl	Microliter
mM	Millimolar
µM	Micromolar
mRNA	Messenger RNA
NaHCO3	Sodium bicarbonate
NaOH	Sodium hydroxide
ng	Nanogram
nk	Normal karyotype
nm	Nanometer
ORF	Open reading frame
PBS	Phosphate buffered saline
PCR	Polymerase chain reaction

Pen/Strep	Penicillin/Streptomycin
pg	Picogram
Ph+	Philadelphia chromosome (t(9;22)(q34;q11)) positiv
pM	Picomolar
PTK	Protein tyrosine kinases
q-PCR	real-time PCR (quantitative PCR)
RING1	Really Interesting Protein 1
RING2	Really Interesting Protein 2
RNA	Ribonucleic acid
RNase	Ribonuclease
rpm	Revolutions per minute
RPMI	Roswell Park Memorial Institute culture medium
RQ	Relative Quantification
RT-PCR	Reverse transcription PCR (cDNA synthesis)
RV	Reverse
SAM	Sterile alpha motive
SCN	Severe Congenital Neutropenia
sec	Second
t	Threshold
Taq	Thermus aquaticus (-Polymerase)
TBE	TRIS-Borat-EDTA-Puffer
TCR	T-cell receptor
TE	Tris-EDTA buffer

TNF	Tumor necrosis factor
TRIAD	Two RING fingers and DRIL
TRIS	Trishydroxyaminomethan
U	Unit
UV	Ultraviolet light
V	Volt
VSN	Variance stabilization and calibration for microarray data
WBC	White blood cells
WHO	World Health Organization
x g	Times gravity

Danksagung

Ich danke meinem Doktorvater Herrn Prof. Dr. med. Bohlander für die Überlassung des Themas meiner Dissertation, die wissenschaftliche Betreuung und Unterstützung bei der Durchführung des Projekts.

Weiterhin möchte ich Frau Dr. Luciana Fontanari Krause für die Einarbeitung danken. Für die weitere Unterstützung, vor allem bei der technischen Umsetzung der Versuche, gebührt großer Dank Medhani Mulaw und Belay Tizazu. Zuletzt danke ich allen Mitgliedern der Arbeitsgruppe dafür, dass sie mir immer mit Rat und Tat zur Seite standen.